



Article

A Multiproxy Approach to the Reconstruction of an Ancient Manufacturing Technology: A Case Study of a Faience Ptolemaic Bowl from Tell Atrib (Nile Delta)

Małgorzata Zaremba ^{1,*}, Jerzy Trzciniński ^{2,*}, Magdalena Rogulska ³ , Grzegorz Kaproń ², Fabian Welc ¹  and Anna Południkiewicz ⁴

¹ Institute of Archaeology, Cardinal Stefan Wyszyński University in Warsaw, Wóycickiego 1/3, 01-938 Warsaw, Poland; f.welc@uksw.edu.pl

² Faculty of Geology, University of Warsaw, Żwirki i Wigury 93, 02-089 Warsaw, Poland; gkapron@uw.edu.pl

³ Department of Polymer Chemistry, Institute of Chemical Sciences, Faculty of Chemistry, Maria Curie-Skłodowska University in Lublin, Gliniana 33, 20-614 Lublin, Poland; mrogulska@umcs.lublin.pl

⁴ Polish Centre of Mediterranean Archaeology, University of Warsaw, Nowy Świat 4, 00-497 Warsaw, Poland; a.poludnikiewicz@uw.edu.pl

* Correspondence: malgorzata.zaremba91@gmail.com (M.Z.); jerzy.trzcinski@uw.edu.pl (J.T.); Tel.: +48-22-569-68-17 (M.Z.); +48-604-779-279 (J.T.)

Received: 22 June 2020; Accepted: 2 September 2020; Published: 5 September 2020



Abstract: Faience objects produced from the fourth millennium BC in ancient Egypt are considered as the first high-tech ceramics in human history. Despite extensive studies on manufacturing technology, many aspects of this complex technology remain a mystery and there is no methodology in place to unravel the techniques of Egyptian faience object production. Detailed studies presented herein fill the gaps, verifying standing opinions and allowing certain aspects of faience manufacturing technology to be reconstructed. The object of this innovative investigation is a hemispherical faience bowl discovered by archaeologists excavating a Ptolemaic workshop district at the site of Tell Atrib in the southern Nile Delta. The multiproxy analysis included the application of specialised software and preparation techniques coupled with complementary methods of light and digital microscopy, SEM with EDS, XRD, STA with EGA, as well as image analysis. Sources of raw and accessory materials (mineral and organic binders, fluxes, colourants) used for preparing the silica paste and glaze slurry were determined. The results helped to reconstruct how the raw material was prepared and how faience vessels were made. The bowl was moulded by compression using a two-part mould. The moulded and dried bowl was then covered by glaze slurry using the application method. A synthetic colourant, Egyptian Blue, was probably used to colour the glaze. The item was fired once at a temperature of 1050–1150 °C. Oxidised conditions were maintained in the kiln during the firing process and firing at the maximal temperature was relatively short. Application of the multiproxy approach has shed light on the technological aspects of faience bowl manufacturing. The obtained results have confirmed the usefulness of the comprehensive methodology that was applied for the reconstruction of particular manufacturing stages of faience objects.

Keywords: Athribis; relief-decorated hemispherical bowls; silica paste; moulding; glaze slurry; glazing; firing; light and digital microscopy; Scanning Electron Microscopy with Energy Dispersive Spectroscopy (SEM-EDS); qualitative and quantitative image analysis; X-ray Powder Diffraction (XRD); Simultaneous Thermal Analysis (STA); Evolved Gas Analysis (EGA)

1. Introduction

The beginnings of faience manufacturing in ancient Egypt go back to the predynastic period in the fourth millennium BC. The manufacturing techniques applied to these unique and exclusive items were modified and improved over the centuries, but significant technological development took place especially in the Hellenistic Period. Several generations of experience and a high level of technical skill were at the source of extremely beautiful faience objects which, however, were highly demanding as far as the manufacturing process is concerned. In the Ptolemaic Period, a plethora of different objects were produced, including vessels, figurines and ornamented items, often displaying complicated shapes and decoration. Relief-decorated hemispherical bowls are of particular interest. They are considered among the most advanced technologically faience objects from ancient Egypt.

Faience objects were produced from silica paste, the main component of which over 90% was fine quartz with admixtures that played various functions during the manufacturing process. Sophisticated techniques were applied to the moulding process. The surface of the objects was coated with glaze, typically blue or green in colour. Glazing flowed the process of decorating the surfaces with relief motifs. Some reliefs were filled with a mixture containing colourants. The objects were fired in kilns of an advanced construction. Application of such a complex process indicates that the faience objects are considered as the first high-tech ceramics in human history [1]. This view is accepted by numerous researchers, e.g., Nicholson and Welch [2,3].

The chemical composition of glaze in faience objects from the Early Dynastic Period to the Hellenistic Period in terms of the colourants used was studied in detail by Kaczmarczyk [4]. Vandiver [5] determined the typical chemical and grain size composition of the body, containing from 92 to 99% of silica and a small admixture of calcium, sodium, potassium, magnesium, titanium, aluminium and copper compounds. Based on optical microscopy studies, she proposed criteria for determining one of the glazing methods used: application, efflorescence or cementation. Scanning electron microscope (SEM) studies of the glazing methods were expanded by microstructural analyses of faience objects and their replicas [6,7]. The investigations of Vandiver and Tite [5,8,9] were focused on silica paste admixtures that maintained its consistency and plasticity. These authors proposed clay or organic binders that enabled moulding of faience objects even on a potter's wheel. For the reconstruction of the silica paste, Matin [10] used *Serish* as an organic binder, which Persian refers to the powdered root tuber of the plant *Asphodelus sphaerocarpus*. The aqueous solution of *Serish* was commonly used in Persia in many traditional handicrafts, e.g., bookbinding and textile crafts [11]. Analysis of quartz pebbles recognised in the Tell el-Amarna and Memphis sites has shown that they were used for faience manufacturing [12,13]. In turn, Shortland [14] interprets the iron and aluminium content in analyses of quartz grain surfaces as the usage of desert sand or pebbles in the preparation of the silica paste. The multiproxy investigations of Mao [15] included detailed structural studies in SEM with EDS and WDS analyses, and X-ray fluorescence analysis, which were preceded by macroscopic observations and xeroradiography. These results are interpreted with regard to the use of forms for the manufacturing of faience objects. An important issue in the reconstruction of the manufacturing technology is the remains of workshops, especially kilns, which were subject to detailed studies in the Tell Atrib, Tell el-Amarna and Memphis sites [16–18].

Faience objects are relatively rare on archaeological sites. These are usually single fragments from poorly dated contexts. Numerous well-preserved faience objects can be found in museum collections all over the world. However, most of them have not been dated and their provenance remains unknown. Despite numerous studies conducted so far, many crucial issues related to faience manufacturing technology have yet to be resolved including:

- Determining of the raw material used to produce faience objects, particularly the admixtures which affected on conditions of moulding and firing;
- Recognition of the structural–textural features of the faience, as well as the relationship between glaze and body;

- Reconstruction of the process of silica paste preparation, relief decorating and glazing;
- Determining the number of firing stages, their temperatures, duration and conditions in the kiln.

The existence of this large number of unsolved issues was a trigger to undertake novel studies on the technology of faience manufacturing. A multiproxy approach was applied, including mutually complementary research methods and detailed textural–structural analyses of the faience material. Interpretation of the obtained results may supply many answers to some of the unsolved issues.

The main focus of the studies was the elaboration and application of a novel and multiproxy analytical method and assessment of its significance in the reconstruction of technological processes applied in faience manufacturing in antiquity. The particular aims include: (1) determining the physical parameters which supply detailed information on the process of silica paste preparation; (2) determining the textural–structural, mineralogical–petrographic and chemical characteristics of the faience body and glaze; (3) determining the parameters of the grain skeleton, matrix and pore space of the faience body; (4) determining the raw material, binders, fluxes and colourants; and (5) determining the moulding and firing conditions.

The set-up aims were achieved by using multiproxy and mutually complementary preparation and research techniques on a macro- and microscale (Figure S1). Observations were made in a digital and optical microscope and in a SEM, analyses of the elemental composition were performed with the application of EDS, the mineral composition was determined using X-ray Powder Diffraction (XRD) analysis, the gaseous composition, using Simultaneous Thermal Analysis (STA), Thermogravimetry–Differential Scanning Calorimetry (TG-DSC) with Evolved Gas Analysis (EGA), Fourier-Transform Infrared Spectroscopy–Quadrupole Mass Spectrometry (FTIR-QMS) and the microstructural parameters were determined using digital image analysis.

The studies were performed on a fragment of a relief-decorated hemispherical bowl from the Tell Atrib archaeological site. The bowl was subject to analyses that were aimed at reconstructing the techniques used during its manufacturing. Following the multiproxy approach, the set-up aims of reconstructing some aspects of faience manufacturing technology were achieved. As a result, the obtained data allowed establishing the properties of the basic raw material, i.e., quartz, and its origin. Analysis of the faience body and the glaze layer allowed drawing conclusions on the applied admixtures which significantly influenced the moulding, drying, glazing and firing conditions. Quantitative image analysis with the application of specialised software led to obtaining raw material parameters crucial for the manufacturing technology, such as grain size distribution and their orientation, or the characteristics of the pore space. Quantitative analyses allowed specifying the qualitative description and supplied strong evidence on the course of some technological processes, such as preparation of the silica paste, its interaction with water and admixtures, moulding of faience objects, and their drying, glazing and firing. Additional important methodological aspect of the performed investigations was establishing the usefulness of the applied research techniques in the reconstruction of subsequent stages of the faience manufacturing technology.

2. Archaeological Site and Faience Object

2.1. The Excavation at Tell Atrib

Studies of Ptolemaic faience manufacturing technology were hampered by the lack of precisely dated artefacts from this period until the discoveries made at the Tell Atrib archaeological site (ancient Athribis), located in Benha in Egypt (Figure 1a). Excavations were conducted first by Kazimierz Michałowski in 1957–1968 on Kom A and then by Barbara Ruszczyc in 1969–1984 on Kom Sidi Yousuf [19–22]. The work was continued by a Polish-Egyptian mission headed first by Karol Myśliwiec in 1985–1995 and then by Hanna Szymańska in 1998–1999 [23–25]. The excavations and multiproxy studies are reflected in numerous publications, e.g., [3,26–30].

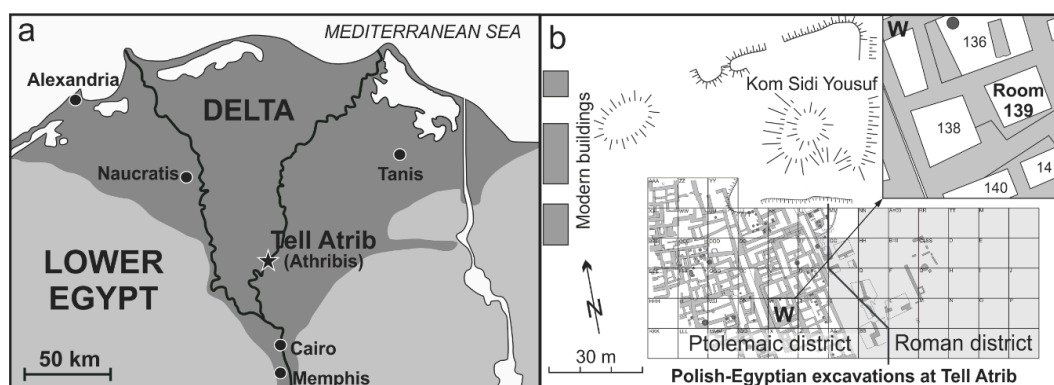


Figure 1. The Tell Atrib (Athribis) archaeological site. (a) Map showing the location of the site in the Nile Delta (Egypt) marked with a star; (b) site map with the location of Room No. 139 in the presumed Ptolemaic faience production area, where fragments of the faience bowl were found.

A fragment of a workshop district with an undisturbed stratigraphic sequence was discovered in the Ptolemaic and Roman parts of ancient Athribis (Figure 1a). A plentiful assemblage of artefacts included numerous terracottas, ceramics and faience objects in successive layers. An absolute and contextual chronology of these layers was established on the grounds of a study of associated coins and stamped handles of imported amphorae [31,32]. In his study of the faience material from these well-dated archaeological contexts (from the second half of the third century until the second century BC), Welc suggested the location of faience production workshops in the Ptolemaic district found south of Kom Sidi Yousuf (Figure 1b). The bowl studied in this article came from Room 139 in the general area of these presumed workshops [3]. Traces of settlement from the Greco-Roman period for nearly two millennia were covered by silty clay sediments of the Nile Delta. Specific water-ground conditions prevailing in this area preserved faience objects in good condition. As a result of extraction from the sediment, many undamaged faience vessels were mechanically damaged during the excavation works. Since the excavation, the faience objects have been kept in museum conditions and were not subject to conservation procedures.

2.2. Relief-Decorated Faience Bowl

Faience manufacturing technology in ancient Egypt reached a peak development in the Ptolemaic Period, between the third and second centuries BC [3,13]. Numerous kinds of faience objects were produced during this time, including vessels, figurines and ornamental pieces. Relief-decorated hemispherical bowls, covered with polychromatic glaze are among the most high-tech items compared to the rest of the faience production. A fragment of a hemispherical bowl (MS) of type B.1 (cat. 4), discovered at Tell Atrib [3,27,33,34], was selected for the purpose of reconstructing the technological process of faience manufacture. The fragment comprises a base with a diameter of 3.5 cm, and the lower part of the body with the wall 0.4 cm thick (preserved dimensions of the sherd: height, 9.3 cm; width, 10.0 cm (Figure 2a). The faience body is composed of low-porosity-fired silica paste, covered with a thin layer of polychromatic greenish-blue glaze. The polychromatic glaze is darker on sunken parts and lighter on the raised relief. This is a typical feature of relief-decorated faience vessels from the Ptolemaic Period [3,13]. The bowl fragment is dated contextually to the second half of the third century [3].

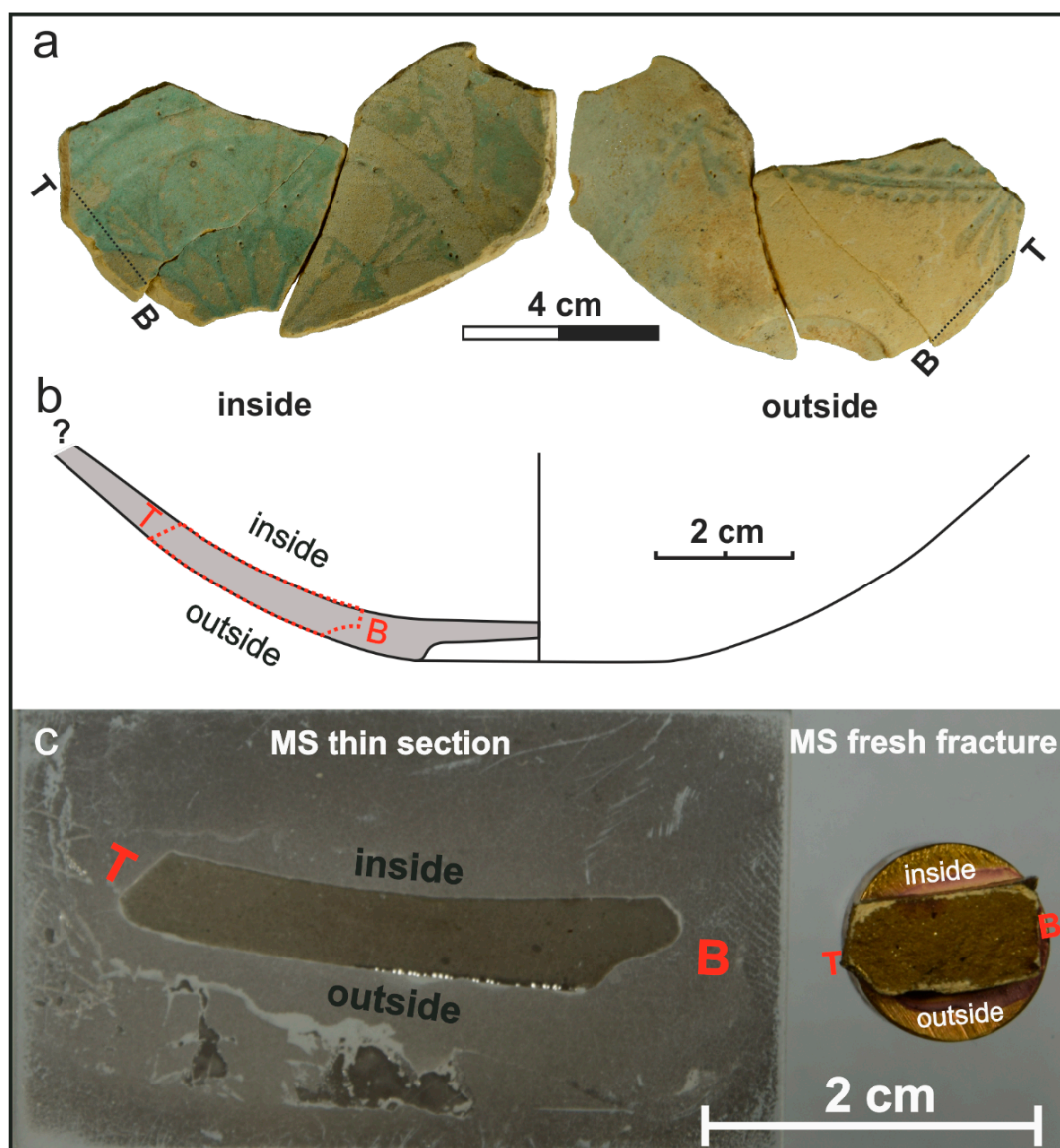


Figure 2. Fragments of the relief-decorated faience hemispherical bowl found at the Tell Atrib archaeological site. (a) Photograph of the analysed fragments. The black dotted line indicates orientation (T—top, B—bottom) of the sample cut out for further investigations; (b) shape reconstruction. The red dotted line indicates the area of the sample used for the preparation of the thin section and fresh fracture; (c) prepared MS samples with marked orientation T–B: MS thin section (left), MS fresh fracture (right).

3. Analytical Methods

Appropriate and detailed recognition of the internal structure of a material and identification of its components requires observations on various detection levels from macro-, through meso-, to microscale, and even down to nano and atom scale. Such an approach allows for obtaining a large dataset which, when combined, results in an overall image of the subject and ensures an appropriate interpretation, e.g., reconstruction of the manufacturing technology of materials and items used in antiquity.

The multiproxy analysis began with the macroscopic observations of the bowl: glaze and body on the vessel walls and on the fracture (Figure S1). Microstructural analysis with the application of microscopic techniques required the preparation of a fresh fracture and a thin section from the vessel fragment. Microscopic observations were performed in a cross-section perpendicular to the vessel wall. The inside wall surface is located towards the upper margin in the presented images. MS samples

(MS thin section and MS fresh fracture) were prepared from a fragment cut out from the faience bowl (Figure 2b,c). Additional preparation was made from the separated fragments of the faience layered structures, and the remaining chips were subdivided into individual samples for the planned analyses.

The MS thin section sample was made on standard microscopic glass, 26 × 48 mm in size. After cutting out a 5 mm thick band, the sample was impregnated with epoxy resin in vacuum conditions. The impregnated sample was glued to glass, and next, the sample was pulverised to the thickness of about 0.025 mm. The surface of the thin section was polished to a smoothness that allowed analysis at large magnifications.

3.1. Digital and Stereoscopic Light Microscopy

Observations of the faience bowl fragments began from macroscale (see Section 4.1). A Delta Optical 450T stereoscopic light microscope with a DLT-Cam PRO camera and a Delta Optical Smart 5MP PRO digital microscope were used for the preliminary analysis. Glaze and relief decorations on the surface and in cross-sections and the body on the fracture surfaces were analysed. Next, the study included precise separation of the layers comprising the faience bowl: glaze layer, interaction layer, relief infillings and body layer. Fragments of each layer were next subject to detailed observations. Mutually differing structural elements and relicts of raw material or firing process were selected for detailed analyses. The separated parts of the faience material were then used to make a preparation for SEM studies (see Section 3.3 for details). The leftover material from particular layers was used in the remaining analyses (see below).

3.2. Polarised Light Microscopy

High-resolution large-format scans allow for the observation and analysis of the material structure of the bulk sample fragment and its parts at variable zoom. Combining such observations with the exact place of sample acquisition from the analysed object permits the determination of correct relationships between the internal structure and material properties with the manufacturing technology. Analysis of the scanned surface facilitates the selection of crucial places that require detailed investigations with the application of other techniques.

The large-format scan of the MS thin section sample was made with the use of a Nikon Eclipse LV100 POL polarising microscope equipped with a DS-5Mc camera and a mechanised Märzhäuser table with high positioning precision in the XY plane. The table allowed for an automatised scan of a series of images and their precise stacking with the use of the stitching mode in NIS Elements. The scan was prepared at ×4 magnification under plane-polarised light (one nicol) and crossed polarised light (two nicols); each surface was composed of 108 images (18 × 6) with a total resolution of 21,694 × 5844 pixels (see Section 4.2.1).

The MS thin section sample analysis was performed with the application of a Zeiss Axioplan petrographic polarisation microscope coupled with a digital camera. The studies were focused on features of the faience texture and structure such as: dimensions of grains and pores, their shape and rounding, distribution of components of the grain skeleton and matrix, and identification of the minerals.

3.3. Scanning Electron Microscopy (SEM) with Energy Dispersive Spectroscopy (EDS)

3.3.1. MS Fresh Fracture Sample

The next step of the analysis was made with the application of a Jeol JSM-6380LA SEM. The analysis was executed in a high vacuum. The fractured sample was gold-coated and observed in the secondary electron (SE) mode. The selected regime of microscopic analysis allowed obtaining images with sharp boundaries between the structural elements (grains and particles) and the pores. The skeleton built of grains, aggregates and particles, the degree of packing, the types of contact between the structural elements, and the pore space were characterised.

3.3.2. Fragments of the Faience Layered Structure

A Jeol JSM-6380LA apparatus integrated with an EDS Bruker GmbH XFlash 6/10 detector was used in the qualitative microstructural characteristics of the layered structure fragments (see Section 3.1). The analysis was performed in low vacuum conditions, i.e., 35–40 Pa, at: acceleration voltage 20 kV, beam current 65 mA, working distance 10 mm, and live time of chemical analysis at 60 s. In such conditions it was not necessary to coat the surface with carbon, therefore no peaks resulting from coating with this element were detected. The photographs were made using the backscattered electrons (BSE) mode. The investigations were made to carry out qualitative analyses of the layered structure and chemical composition of the faience object.

3.3.3. MS Thin Section Sample

A carbon-coated thin section was observed with Zeiss Sigma™ VP (variable pressure) SEM with a field emission electron gun (FEG) using the AsB™ (Angular selected BSE) detector and EDS analyser using CrossBeam® Technology EDX (XFlash 6/10™) detectors produced by Bruker GmbH. The chamber design provides an ideal geometry for simultaneous two-detector EDS analyses. The analysis was executed in a high vacuum at an acceleration voltage of 20 kV, beam current of 80 μ A, working distance of 7.7 mm and live time of chemical analysis at 60 s. The investigations were aimed at qualitative analyses of the faience layered structure and the quantitative analysis of its chemical composition.

3.4. Image Analysis

The analysis was executed with the application of a Jeol JSM-6380LA SEM in a high vacuum. The MS thin section sample was viewed in a backscattered electron (BSE) mode after coating with a layer of carbon. Photographs were used to carry out image analysis. Quantitative image analysis was based on BSE images with the application of specialised STIMAN (STructural IMage Analysis) software [35–38]. Morphometric and geometric parameters of the pore space and the grain skeleton were determined. The analysis was performed on a series of images at $\times 50$, $\times 100$, $\times 200$, $\times 400$, $\times 800$, $\times 1600$ and $\times 3200$ magnifications, on the total area of 5 mm², following the software instruction [37].

Analysis of SEM images allowed determining the following parameters: area S , perimeter P , diameter D , form index of the pores and grains K_f , and degree of orientation, anisotropy, K_a of the structural elements. The obtained distribution of the equivalent diameter of the grains allowed determining the abundance of the grain fractions and drawing a grain size distribution curve. Based on the distribution of the equivalent diameter of the pores, the contents of ultrapores, micropores, and mesopores were determined [39]. The form index K_f allowed distinguishing three categories of pores and grains [37]: isometric, anisometric, and fissure (pores) or elongated (grains). The degree of orientation of the structural elements was determined following the method of gradient intensity signal [40,41]. The obtained pie-chart, orientation rose, was used to determine the values of microstructural anisotropy K_a and the preferred orientation direction α of the structural elements [41].

3.5. X-ray Powder Diffraction (XRD)

X-ray Powder Diffraction (XRD) was performed for the MS sample: glaze together with the underglaze layer (MS-GLZ) and the body layer (MS-BDY) separately (see Section 3.1). The samples were analysed with an X'Pert PRO MPD (Panalytical) diffractometer using Co K α radiation, in the same range of 2θ , with a step of 0.026° 2θ . The Bragg–Brentano method and the DSH method (Debye–Scherrer–Hall) was applied for analyses of the MS samples. The first one requires about 400 mg of the powdered sample, whereas the second one requires 20–30 μ g. The MS-BDY sample was analysed with the Bragg–Brentano method with the registration time of 3 h and 4 h and the MS-GLZ samples were analysed with the DSH method with the registration time of 1 h and 3 h, respectively.

3.6. Physical Properties

A fragment of the faience bowl covered with glaze, with a volume of about 1 cm^3 (2 cm^2), was used to determine the specific and bulk density. To determine bulk density, the surface of the faience material was sealed with parafilm. Bulk density was determined using the water displacement method according to [42]. The AS 110.R2 PLUS Analytical Balance with KIT 85 Density Determination Kit for determining the density of solids and liquids was applied. The parameter was designated based on two determinations. Studies of specific density were performed with the application of a helium gas pycnometer. The same faience fragment was ground in an agate mortar to a fraction below 0.1 mm. Before determination, the sample was dried at a temperature of $105 \text{ }^\circ\text{C}$. The AccuPyc 1330 model was used in the determinations and the analysis was performed according to the operating instructions. The parameter value was designated based on 50 determinations and used to calculate the porosity value and the void ratio.

The porosity of the material was also determined with the application of a second method, STIMAN software, based on the quantitative analysis of SEM images (see Section 3.4). The void ratio was based on calculating the relationship between porosity and the void ratio.

3.7. Simultaneous Thermal Analysis (STA): TG-DSC with Evolved Gas Analysis (EGA): FTIR-QMS

TG-DSC was performed for the MS sample: glaze and underglaze layer (see Section 3.1 for sample preparation), by means of a Netzsch STA 449 Jupiter F1 instrument (Germany) in a helium atmosphere (flow rate at $20 \text{ cm}^3/\text{min}$), from room temperature up to $1000 \text{ }^\circ\text{C}$ at the heating rate of $10 \text{ }^\circ\text{C}/\text{min}$. The TG-DSC analysis was conducted in a crucible made from Al_2O_3 . The mass of the sample was 30 mg. At the same time, gaseous FTIR and QMS spectra were gathered by an FTIR TGA 585 (Bruker, Germany) and QMS 403C Aëolos (Netzsch, Germany) analysers in order to evaluate the gaseous products emitted during heating of the tested compound. The FTIR spectrometer with the IR cell kept up at $200 \text{ }^\circ\text{C}$ was connected online to an STA apparatus by a Teflon transfer line with a diameter of 2 mm heated to $200 \text{ }^\circ\text{C}$. The FTIR spectra were recorded in the spectral range of $4000\text{--}600 \text{ cm}^{-1}$ with a 4 cm^{-1} resolution and in 16 repetitions. The QMS analyser was connected online to an STA instrument by a quartz capillary heated to $300 \text{ }^\circ\text{C}$. The QMS was operated under electron ionisation with an energy of 70 eV. The QMS measurement in scan mode for m/z , where m is the mass of the molecule and z is the charge of the molecule in electron charge units in the range of $1\text{--}100 \text{ } m/z$ was performed.

4. Results and Interpretation

4.1. Digital and Stereoscopic Light Microscopy

Observations of the faience bowl fragments using digital and optical microscopy are presented in Figure 3 and Figure S2. Threefold enlargement of the bowl fragment allowed observing the faience structure composed of a thin glaze layer, a body layer and relief decorations (Figure 3a–c). The glaze is greenish-blue in colour with a thickness of about 0.3–0.4 mm. Glaze preservation of the analysed fragments is variable. It is best preserved on the inside of the bowl fragment, whereas on the outside, it occurs mainly in the sunken parts of the reliefs (see Figure 2a). The glaze surface is covered by numerous oval depressions (holes), 10 to 20 μm in diameter, and a network of canaliculi, which are visible at $\times 45$ magnification and do not display any orientation (Figure 3e and Figure S2a,d). Dark brown relicts of glaze slurry are visible in some pores within the glaze (Figure 3f and Figure S2b,d). The interaction layer can be found between the glaze layer and the body layer; it was exposed during sample preparation for further studies (Figure 3f). This layer is characterised by high transparency and a lighter colour than the glaze. It is even colourless in places. A much larger number of pores was determined within compared to the glaze surface and interior. The body is yellowish-white in colour, attaining a light orange hue directly below the glaze layer (Figure 3f and Figure S2c,d). The body thickness is about 3–4 mm and thins out towards the bowl rim. Apart from a homogenous mass, a $\times 15$ magnification of the body surface displays larger grains, 0.1–0.2 mm in size (Figure 3c).

The grain colour is uniform; white and transparent grains prevail, whereas pink and grey grains are rare. A $\times 45$ magnification of a fragment of the body surface shows a linear orientation of elongated quartz grains, whose longer axes are arranged parallel to the vessel walls and directed according to the T–B orientation (Figures 2b,c and 3d). The body also contains round and oval pores of variable sizes. Dimensions of the largest ones reach even 1 mm (Figure 3b). The internal walls of large pores are characterised by smooth surfaces. The longer axes of oval pores are oriented parallel to the vessel walls and follow the T–B orientation. The body also contains transparent elements resembling a ribbon, whose length reaches 1 mm and width does not exceed $10\ \mu\text{m}$ (Figure S2b,d). The body surface is covered by reliefs (Figures 2a and 3a,b), which are 0.3 to 0.6 mm deep and filled with light brown silica paste that has a higher porosity than the body. The infilling mass does not adhere tightly to the body surface, forming small voids, 0.2 mm in size. In turn, it is attached well to the covering glaze layer.

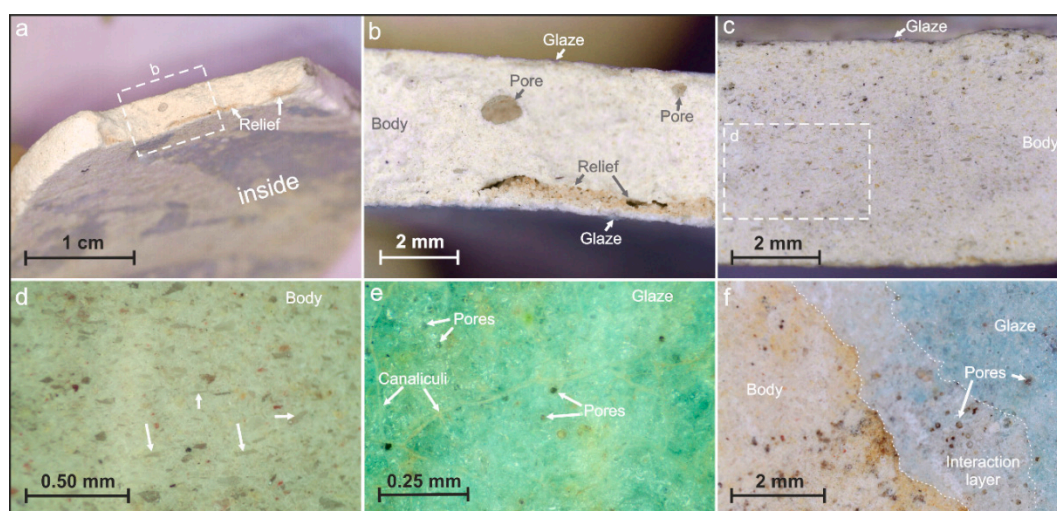


Figure 3. Layered structure of the faience bowl observed under a digital and light microscope. (a) Fragment of the faience bowl with reliefs; (b) fragment of fresh fracture marked on (a). Glaze layer, oval pores in the body and relief (hollow underglaze with filling) are visible; (c) fragment of the area after cutting of the sample. Orientation of the photograph T–B (B—right side, see Figure 2). Glaze layer and grains in the body characterised by different colours, sizes and shapes are well-visible; (d) fragment of the area marked in (c) with the well-visible orientation of elongated quartz grains (arrowed); (e) glaze surface with well-visible pores and canaliculi (arrowed); (f) fragment of the inside surface of the faience bowl. Glaze layer visible in the upper right side of the image, below the partly exposed interaction layer and body layer. Well-visible dark grains in the body and oval pores in the glaze and interaction layer. (a–c,f) show images taken under a digital microscope, (d,e) show images taken under a light microscope.

Selected structural elements observed during the analyses were used to prepare a sample for further studies (Figure S2). Their analysis supplied new data on the processes taking place during firing of the faience object (see Section 4.3.2).

Interpretation

Degassing of the forming alloy must have begun during the firing process, as evidenced by pores located in the glaze and in the interaction layer. The formation of these pores could also depend on the degassing of the body layer during a single firing. The presence of pores may indicate the faience firing temperature but this requires detailed investigations (see Section 4.7). The degassing bubbles derive from gas imprisoned between the melted particles of the powdered glaze slurry. Bubbles reaching the surface from the melted glaze formed depressions similar to pin-holes [43]. The canaliculi network observed in the glaze developed during the firing process. Canaliculi formation

is linked with diverse thermal expansion of the body and glaze layer. Formation of the canaliculi required a coefficient of the thermal expansion of the glaze layer (continuous layer) higher than the sum of the values of this parameter for quartz grains of the body layer (discontinuous layer; for an explanation, see Section 4.3.3). Tensile stress develops when the glaze shrinks more intensely than the body during cooling. Large stress values may cause the development of cracks in the glaze. A fracture network resembling a spider-web pattern was formed on the surface; it is similar to that observed on glazed pottery, where it is referred to as crazing [44].

The low content of large quartz grains in the body points to good fragmentation of the material. Angular elongated grains indicate that crushed quartz rocks were used for manufacturing the bowl. The orientation of elongated quartz grains and elliptical pores indicates that moulding methods including compression of the silica paste must have been used in the manufacturing process. A small content of air was trapped in the material during moulding of the silica paste. During compression, the air concentrated in the form of oval bubbles, whose shape became slightly flattened along the direction of tensile force and perpendicular to the compressive force. Therefore, orientations of the longer pore axes are in accordance with the T–B orientation. Fine elongated quartz grains followed the shape of the bubble surface because of the pressure within the bubble. After drying, the distribution of grains reflecting the bubble shape was preserved due to mineral and organic binders, and after firing the smooth surface of the pores became fixed. Ribbons found in the body were formed during the firing process. Their bent shape is the effect of creating new phases between the quartz grains. The reliefs were infilled with a slightly different material than the silica paste used for the moulding of the body, as indicated by the different colours and larger porosity of the relief infilling. The colourant used for relief infilling must have been earlier mixed with glue. The large porosity of the relief infilling material is the result of burning organic matter from the glue.

4.2. Polarised Light Microscopy

4.2.1. Analysis of the Large-Format Scan

A large-format thin section scan was used to analyse a large fragment of the faience bowl cross-section with a surface area of about 2.5 cm² (Figure S3). The body layer (BDY) with light grey quartz grains in a dark brown matrix and the glaze layer (GLZ) and interaction layer (IAL) are well-visible on the plane-polarised light (one nicol) image (Figure S3a). In turn, quartz grains (light blue to dark grey) and single grains of other minerals, e.g., feldspars, and pores (black) can be seen in cross-polarised light (two nicols; Figure S3b). A distinct thin glaze layer, 0.1–0.2 mm thick, with quartz grains within, can be seen at image magnification. A thin, light brown interaction layer (IAL), 0.2 mm thick, is visible below the glaze layer. The glaze layer is about 0.4 mm thick in the hollow observed in the upper right corner of the thin section. The body layer is composed of well-sorted angular quartz grains with sizes below 0.2 mm. Grains larger than 0.2 mm are very rare. The orientation of elongated grains is clearly visible on most of the thin section surface, particularly in its central part; the longer axes of the grains are arranged parallel to the vessel walls, according to the T–B orientation. In some places, the orientation becomes undulated and turbulated (see area close to the bowl's inside wall) or does not occur at all (see area close to the bowl's outside wall). Places of denser material within the body can be seen e.g., in the left lower and right upper corner of the cross-section and in some places in the central part of the thin section. In some cases, lower density areas can be observed, especially in the central parts of the sample area. Large circular and oval pores of variable sizes, from 0.3 to 0.5 mm, are well-visible in cross-polarised light (two nicols; Figure S3b). Similar to the elongated grains, the oval pores are arranged with their longer axes according to the T–B orientation.

4.2.2. Petrographic-Mineralogical Analysis

The matrix, which plays the role of a binding agent, comprises about 10–20% of the analysed faience body. It is an aphanitic, locally very fine-grained, homogenous substance, light brown in colour

(Figure 4). The substance is composed of products of the transformation of clay minerals and other fine-grained components due to firing in high temperatures. Determination of the content of clay minerals is very difficult because they are masked by other components, particularly by the brown ferruginous colourant.

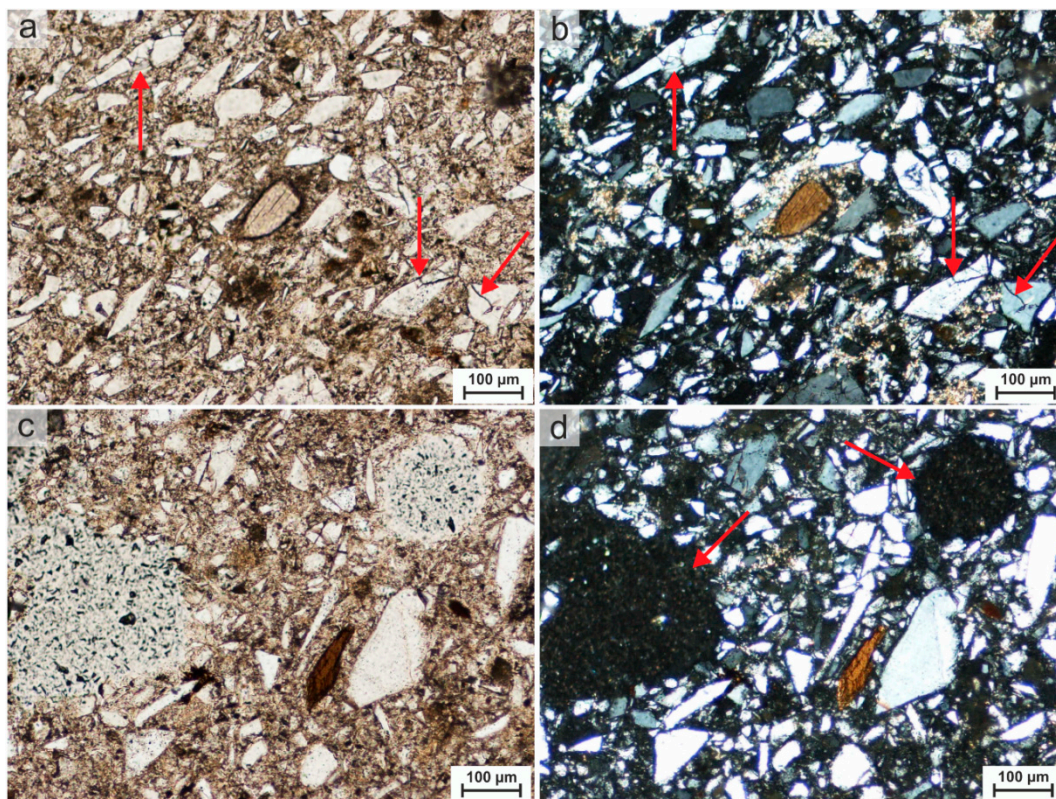


Figure 4. Microstructure of the faience body observed under a polarised light microscope (MS) thin section. Orientation of the photograph T–B (T—lower left side, B—upper right), see Figure 2. (a) Angular quartz grains (white) within the light brown matrix. Arrows indicate fractured grains. Oval light brown pyroxene grain visible in the centre (1 nicol); (b) angular quartz grains (white, light blue, dark grey-blue) within the brown matrix. Well-visible light brown pyroxene grain in the centre. Arrows indicate fractured grains. The same fragment as in (a; 2 nicols); (c) very fine-grained substance with a high degree of homogenisation and light brown colour (matrix) visible between quartz grains. Substance composed of products of thermal alteration of various primary minerals, mainly clay minerals. Its brown shade results from the presence of dispersed, very fine-grained iron compounds, mainly hematite (1 nicol); (d) oval pores (arrowed) and dark brown biotite well-visible. The same fragment as in (c; 2 nicols). (a–d) show well-oriented elongated quartz grain (from upper right to lower left side).

Detrital components (grains) comprise about 80–90%. Their size is very variable, but they are dominated by grains in the coarse aleuritic (coarse silt) and fine psammitic (fine sand) fractions with an average size of about 20 µm. Subordinately occur larger psammitic (sand) grains with a maximum diameter of up to 100 µm. Angular quartz occurs almost exclusively in the analysed vessel fragment; it shows traces of melting. Some quartz grains are slightly cracked. Quartz is typically monocrystalline, whereas the polycrystalline variety occurs very rarely. Other detrital components occur in trace amounts; they are mainly individual crystals of slightly degraded biotite with poor, relict birefringence and pale brown pleochroic colours (Figure 4c,d). Grains of pyroxene have also been noted in the sample (Figure 4a,b). Most quartz grains are elongated, due to which their oriented parallel arrangement is evident.

Interpretation

Elongated and angular quartz grains observed macroscopically were confirmed in petrological observations. The lack of rounded grains excludes the use of sand deposits as raw material. Good sorting points to the selection of the material during the preparation of the mixture. The distinct orientation of the elongated grains as well as the flattening of pores indicate moulding of the object through compression. The variable density of the silica paste and the changing orientation of elongated grains may suggest moulding with a still lower part and a moveable upper part. The uneven clamp during bowl moulding and its bent shape resulted in a variable state of stress and strain in the material caused by the activity of compressive and tensile forces.

The main components of the matrix are clay minerals, partially thermal transformed to very fine-crystalline mullite. The basic component of the grain skeleton is quartz and determination of the rock used as the raw material is not possible at this stage of investigations. Subordinate occurrences of biotite and pyroxene particles may point to magmatic or metamorphic rocks. Variability of the quartz fractions, its poor rounding degree and oriented arrangement point to processes of breaking up of the raw material and silica paste formation. Fine quartz grains display traces of partial melting of the edges, but it is not possible to precisely state the duration and temperature of the firing process.

4.3. Scanning Electron Microscopy (SEM) with Energy Dispersive Spectroscopy (EDS)

4.3.1. Microstructure—MS Fresh Fracture

The analysed faience body is composed mainly of poorly sorted quartz grains. Most grains vary in size from 200 μm to even below 5 μm (Figure 5a,c). The largest grains maximally contribute to 5%. The dominating grains are between 200 and 50 μm and between 40 and 10 μm in size. Edges and corners of all grains are completely nonrounded and highly angular (Figure 5b,c). The edges and corners are partly melted. Melting is more intense and the edges are more rounded in the case of smaller grains. Microporosity between the grains is dominated by pores from 20 to a few micrometres in size. Larger oval pores, attaining diameters of 50 μm and above, are rare. Large and medium grains constitute the base of the grain skeleton, between which occur partly melted, very fine grains (Figure 5c,d).

Interpretation

Partial thermal melting of the edges and corners of the quartz grains forming the vessel body suggests that the firing process was very well controlled. Partly melted parts of the grains attain the form of concave surfaces, which suggests the beginning of a deliberately interrupted melting process. Firing temperature and duration were matched carefully to assure melting only of the fine grains and formation of a firm body.

4.3.2. Microstructure and Elemental Composition—Fragments of the Faience Layered Structure

Single, oval and shallow hollows with sizes from 50 to 100 μm and many similar hollows with smaller sizes below 10 μm can be observed on the glaze surface (Figure S4a, spherical pores (SP)). Similar spherical forms occur within the glaze (see upper left part of the image). Silicon is the main component of the glaze. They are accompanied by carbon, aluminium, chlorine, calcium and lead. Sodium, magnesium, sulphur, potassium, iron and copper occur in trace quantities (compare Figure S4a,b with Table S1). Remains of the glaze slurry, usually represented by alloys with oval, rarely irregular shapes are visible in the upper right part of the image (Figure S4a, ALY, spherical shaped alloy (SSA)). The alloys are rich in metals (Pb, Fe, Cu), alkaline elements (Na, Mg, Al, Ca), as well as carbon, phosphorus, chlorine and sulphur. Oval alloy forms are more common in the glaze and underglaze layers. Single quartz grains, 50 to 150 μm in size and with rounded edges and corners, have been noted (Figure S4a, dark grey, quartz (Q)). Chemical analyses have indicated the presence of small amounts of carbon.

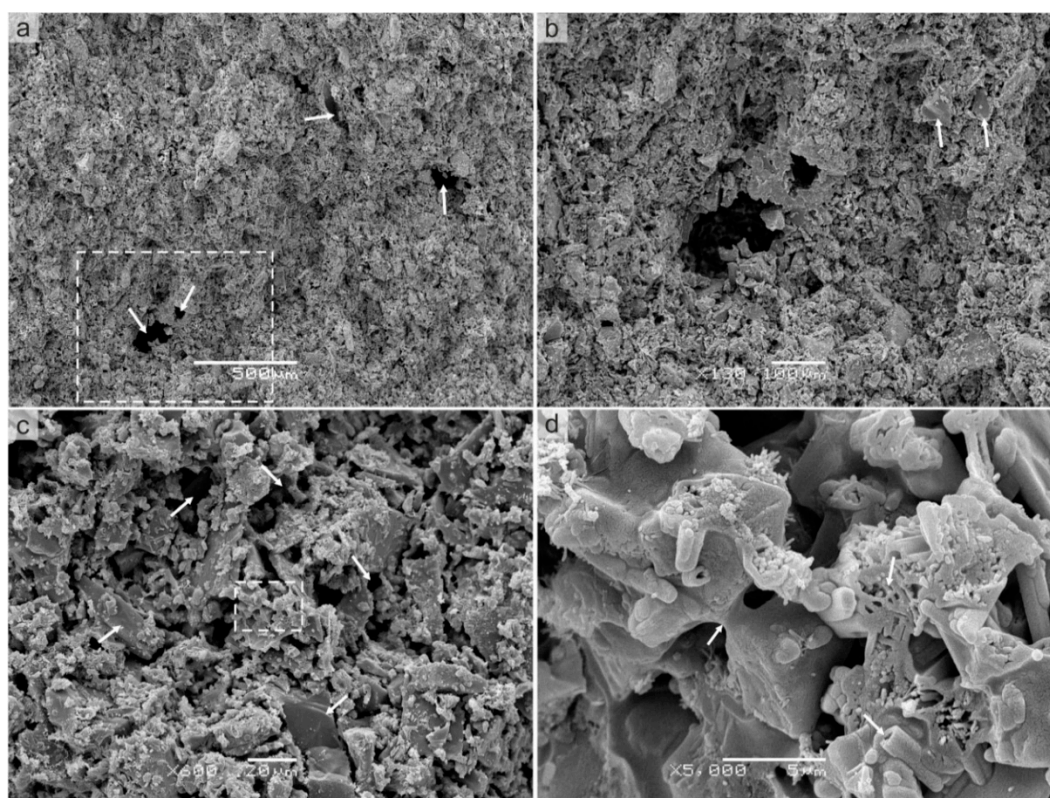


Figure 5. Microstructure of the faience body observed in a scanning electron microscope (SEM)–MS fresh fracture. Images of fracture in the secondary electron mode (SE). White rectangles in (a,c) denote the areas enlarged in (b,d), respectively. Orientation of the photograph T–B (B—right side, see Figure 2). (a) Poorly visible quartz grains surrounding the fine-grained matrix with clay particles. Oval macropores (black area) marked arrows. Scale bar equals to 500 μm indicates a $\times 50$ magnification; (b) well-visible oval macropore in the centre and angular, elongated quartz grains (arrowed); (c) well-visible very fine-grained matrix with clay particles and numerous micropores between fine quartz grains (arrowed); (d) melted quartz grains, particularly well-visible in the centre. Left arrow indicates melted and cemented contact between two fine quartz grains. Well-visible new phases crystallised on the surface of the quartz grains (right upper and lower arrow).

The glaze surface is covered by canaliculi (CL), which form irregular polygons, whereas cracks are rarer (cracks (CR); Figure S4a). The canaliculi attain diameters from 5 to 10 μm and have smooth edges, whereas the cracks are very narrow (1–2 μm) and have sharp margins (see also Figure 3e).

The glazed bottom looks similar to the glaze surface (Figures S4c,e and S5a). Oval degassing pores (SP) and remains, usually alloys after the glaze slurry, prevail in the lower part of the glaze layer (alloys (ALY), SSA). The chemical composition of ALY and SSA is similar, with the largest contents of carbon and silicon. The contents of calcium, sulphur, lead and phosphorus are lower. Compared to SSA, ALY contains less alkaline elements—sodium and magnesium (Figure S4d and Table S1). Pores filled with a fine dispersive substance, probably a relict of glaze slurry (RS) have also been noted. They usually attain an oval form and have a variable preservation and chemical composition. The main elements occurring in the RS include carbon and silicon, enriched in iron and alkaline elements. Phosphorus, chlorine and sulphur occur in small quantities (compare Figure S4c,d with Table S1). Some RS are spherical, strongly porous and contain a very fine dispersed material composed mainly of clay minerals (CLY; Figure S5b,d). Other RS are more irregular with fine particles and coarse grains, and are very compact. They have a variable chemical composition (compare Figure S5c,e with Table S1). All RS contain carbon and silicon, and in variable proportions aluminium, magnesium,

potassium, calcium and iron. They contain also trace quantities of sodium, phosphorus, sulphur, chlorine and titanium.

The body layer structure contains relicts of admixtures to the silica paste (Figure 6a–c). They usually form concentrations (relict of silica paste (RSP)) and alloys (ALY) of the silica paste with irregular shapes lying between the quartz grains (see also Figure 3f). Alloys in the body layer are characterised by a higher content of lead, phosphorus and sulphur than the alloys in the glaze layer, whereas the quartz grains also contain trace amounts of carbon (compare Figure 6a,d with Table S1). Relicts of the silica paste contain dispersed, fine grains of metals and heavier elements sticking in the fine detrital mass, mainly particles of clay minerals. Besides silicon, aluminium and carbon, the chemical composition of the clay minerals from the body includes iron, calcium, potassium, magnesium, phosphorus and trace amounts of sodium. Trace amounts of sulphur, chlorine, titanium and lead have also been noted. Compared to the composition of clay minerals from the RS in the glaze, they contain larger amounts of calcium, phosphorus, sulphur and chlorine. Single platy microaggregates of clay minerals are almost intact.

The body also contains relicts after the firing process in the form of elongated carbon–silicon ribbons (compare Figure S2b,d with Figure 6e–g, C-Si ribbon (RBN)). Their length reaches maximally several hundred micrometres and width does not exceed 10 µm. The ribbons are primarily composed of carbon and silicon. Analysis No. 38 shows also the low content of other elements such as sodium, potassium and calcium, which stands out from the rest of the analyses (compare Figure 6h with Table S1).

Interpretation

These oval hollows are interpreted as pin-holes and were formed during the melting and degassing of products within the glaze slurry (Figure S4a, SP). Pores filled with gas emanated outside from the liquidised glaze. Assuming a single firing process, firing products were also degassed from the body layer, which was surrounded by glaze from both sides. Oval alloys are remains of unreacted substrates of the glaze slurry, which concentrated during firing and solidified after cooling. Their oval form is the result of higher elasticity of the thin and mostly warmer fluid alloy surrounded by a dense and relatively cooler fluid glaze. Cylindrical shapes of quartz grains indicate partial melting of the grain edges following interaction with the molten and fluid glaze. Grains jutting out from the glaze derive from the body surface from which, being poorly bound, they were detached during application of the glaze slurry. This fact points to the application method of glazing. Poorly bound grains on the body surface probably indicate a single firing. Such an approach to the firing process is more practical and economical.

The canaliculi are related to the larger shrinkage of the cooling glaze on the surface of a stiffer body (Figure S4a). They may also be connected with the degassing of the firing products. The dual nature of the canaliculi is linked with gradual cooling and hardening of the interior glaze layer in relation to the quick cooldown of the exterior layer. The cracks, in turn, point to brittle cracking and formation in a stiff glaze layer.

Pores filled with a fine dispersive substance represent relicts of the glaze slurry (RS), whose infilling is almost intact (Figures S2b,d, S4c,e, S5a,b,d). They are preserved in the fired faience material. Explaining the preservation of such forms during firing remains an open question; their detailed studies should supply data on the preparation of the glaze slurry and the glazing process. The increased content of various types of alloys (SSA, ALY) directly below the glaze layer is caused by the sinking of these substances and their preservation of grains of the body layer. The substances, when heavier and warmer, gravitationally sink into the denser and fluid glaze. The inward sinking is linked with the location of the glaze layer from the inside of the bowl and points to the position in which the object was fired.

grains during body moulding and after its drying, and partial infilling of the pore space. Additionally, the organic binder supplied carbon to the reactions taking place during the firing process. After firing, the substance disappeared from the pores, the objects gained high porosity and became very lightweight. The application of an organic binder again points to a single firing stage. In order to state which organic substance was the binder used in faience manufacturing, these structures need to be studied in detail. Additional data on the firing products were obtained from EGA analysis during STA; they have not, however, supplied a comprehensive answer to this issue (see also Section 4.7).

4.3.3. Microstructure and Elemental Composition—MS Thin Section

The thin section displays the faience layered structure, composed of a glazed layer, body layer and an interaction layer between them, which binds both layers (Figures 7 and 8, Figures S6 and S7). The results of the quantitative analysis of the elemental composition are given in Table S2.

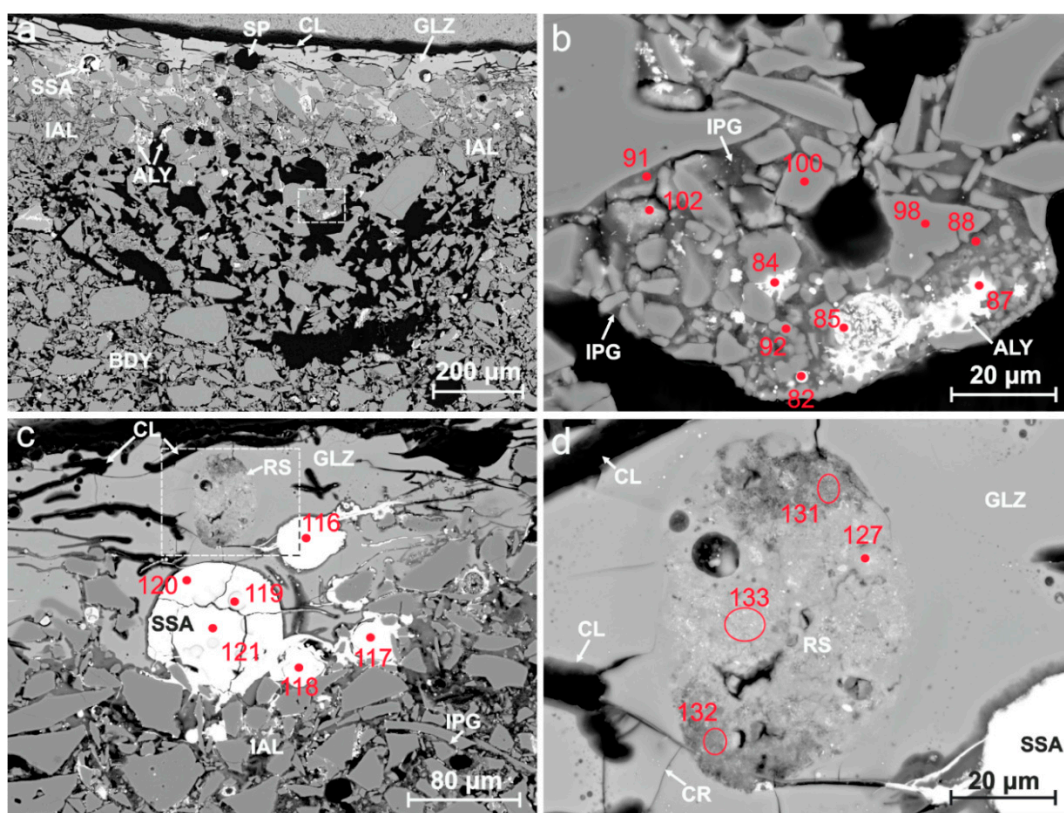


Figure 7. Microstructures of the faience glaze and underglaze layer observed in scanning electron microscope (SEM)—MS thin section. Images viewed in a high vacuum mode (HV) and backscattered electron mode (BSE). Localisation of EDS analysis marked with red number and dot or oval (see Table S2). Orientation of the photographs T–B (B—right side, see Figure 2). (a) Fragment of the body with glaze and underglaze layer. Well-visible canaliculi (CL), spherical pores (SP) and spherical shaped alloy (SSA) in the glaze layer (arrowed). Many fragments of the alloy (ALY) are visible in the underglaze between the interaction layer (IAL) and body layer (BDY). Large fragment of the highly porous body is visible below the glaze and underglaze layer. Highly porous fragment of the body has an oval shape in the bottom and is flat on the top. Notice very fine quartz grains linked by interparticle glass forming a fragile structure inside the porous fragment. White rectangle denotes the area enlarged in (b); (b) fragment of the highly porous body with melted very fine grains of quartz. Alloy and interparticle glass (IPG) existing between the melted grains (arrowed); (c) many spherical shaped alloys (SSA) are visible between the glaze and underglaze layer. Canaliculi in glaze, interaction layer and interparticle glass are well-visible (arrowed). White rectangle denotes the area with a relict of glaze slurry (RS) enlarged in (d); (d) relict of glaze slurry and canaliculi are visible in the glaze layer.

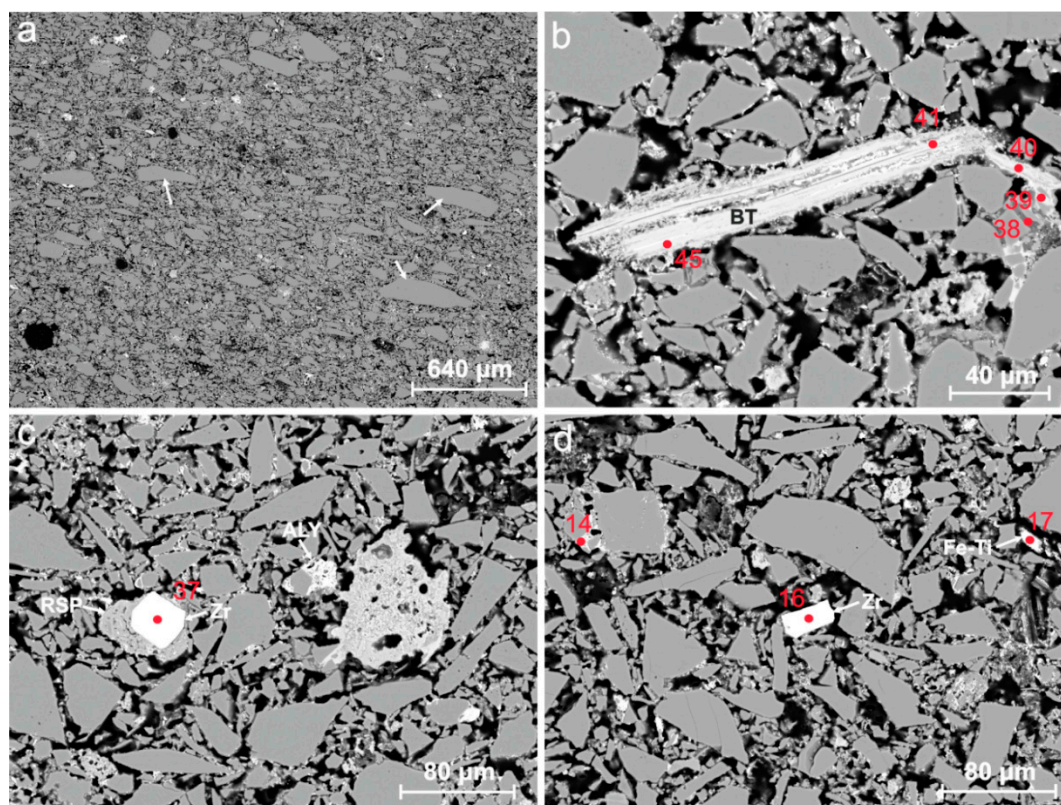


Figure 8. Microstructures of the faience body layer observed in the scanning electron microscope (SEM)–MS thin section. Images viewed in a high vacuum mode (HV) and backscattered electron mode (BSE). Localisation of EDS analysis marked with a red number and dot (see Table S2). Orientation of the photographs T–B (B—right side, see Figure 2). (a) High orientation of elongated quartz grains (arrowed). Well-visible oval pores (black area) with a smooth internal surface; (b) biotite sheets (BT) between quartz grains; (c) fragment of the body with Zr mineral and alloy (ALY; in the centre—arrowed). Relict of silica paste (RSP) surrounding a zirconium mineral (Zr). Note large grain of slag mixed with alloy (on the right); (d) fragment of the body with zirconium (Zr) mineral (in the centre) and iron titanium mineral Fe-Ti (in the upper right).

Glaze Layer

The glaze layer (light grey) tightly covers the body layer (Figure 7 and Figure S6, GLZ). The glaze surface is smooth with small chips. Its thickness is maximally 200 μm (0.2 mm) with insignificant variations. The layer is not homogenous. Its upper part contains single quartz grains sticking in the glaze or slightly jutting above its surface (Figure 7a and Figure S6a, Q). The grain sizes vary from 20 to 100 μm . The grains immersed in the glaze have rounded edges and corners, and the contact zone between the grains and the glaze is blurry (Figure 7a,c). The lower part is fused on the surface of the body layer (BDY), penetrating between the quartz grains (grey) at about 50–80 μm . The lower contact of the glaze is sharp, uneven and has a lighter hue from the rest. Numerous oval pores of variable sizes (Figure 7a and Figure S6b,c, SP) occur in the glaze layer. Large single pores with sizes from 20 to 50 μm are rare. In turn, pores with dimensions from below 10 μm to the tenth parts of a millimetre occur in accumulations (Figure S6c,d). Very fine pores are also present in some quartz grains in all layers. The glaze layer is cut by numerous canaliculi, usually parallel to the surface, rarely perpendicular or oblique (Figure 7a,c and Figure S6a,b). Their length varies from tens to hundreds of millimetres, and the width is from 5 to 10 μm . They occur isolated or in series, forming blind branches. They are oblique and often terminate with a circular thickening. They are usually empty, in some cases only filled with a light grey or white substance. The canaliculi margins are rather blurry and surrounded by a darker edge similar in hue to the glass phase. The edge follows the shape of the canaliculi margin.

The glaze layer contains oval aggregates about 50 μm in size (light to dark grey in colour; Figure 7c,d, RS). The aggregates are inhomogeneous, and have a sharp contact with the glaze in some cases and a blurry contact in others.

A large, oval hollow with a depth of 350 μm , narrower from the top (270 μm) and wider at the base (800 μm), partly filled with glaze, is visible in the body layer (Figures S6c,d and S3a). The glaze surface is concavely curved to the width of the wider, basal part of the hollow, forming an internal, 140 μm deep depression. The glaze layer is covered by cracks and canaliculi. The cracks have sharp margins and terminations. They are up to 200 μm long and about 1–2 μm wide. The canaliculi margins and terminations are cylindrical, their width varies from 5 to 10 μm and length exceeds 250 μm . The cracks and canaliculi have similar patterns, perpendicular and parallel to the upper and lower margin of the hollow (Figure S6c,d, CL, CR). The direction of canaliculi propagation from the body layer and IAL to the surface is clearly visible. Numerous smaller, parallel canaliculi propagate from the main perpendicular canaliculi; their dip is similar to the arrangement of the hollow margins. Moreover, glaze infilling the hollow contains a large number of oval pores, with dimensions from several to 30 μm , and two large pores, with dimensions of 60 μm and 140 μm , respectively. Relicts of material in variable forms are visible in one of the pores. In the lower part of the glaze and directly below occur oval concentrations (SSA) even up to a size of 50 μm . At the contact between the glaze and body, a vast glass layer forming IAL is visible, particularly on the right side. The width of this layer is about 80 μm and it has an uneven surface. A small (up to 10 μm in size) oval concentration with a crack in the middle (RC) occurs in the glaze at the contact with glass. Light-coloured edges concentrically extend from this concentration.

Numerous oval concentrations SSA (white) with variable sizes from 10 to 100 μm can be observed at the glaze and IAL contact (Figure 7c and Figure S6a,b, SSA). The concentrations are inhomogeneous and some of them display internal structures and cracks (Figure 7c and Figure S6d). Similar oval concentrations very rarely occur in the body layer. Oval pores partly infilled with a similar substance have been noted (Figure S6b). Some canaliculi are connected with the oval concentrations and infilled with the same substance. At the IAL and BDY contact occurs an accumulation of concentrations (white) characterised by irregular shapes (Figure 7a,b, ALY).

The elemental composition of the glaze layer is homogeneous (Table S2, GLZ). The basic component is silicon (about 45%). Among alkali, calcium (3–5%) dominates above potassium (0.5–1.5%). Magnesium occurs in low quantities up to 0.5%, whereas sodium is not detected. The content of lead in the glaze is about 5–6%; chlorine, 3–4%; iron, 1–2%; and copper, up to 2.6%. Aluminium, titanium and barium occur in trace quantities. Analysis No. 1 shows the lack of lead and a significant decrease in the contents of iron, copper and calcium. In turn, the contents of magnesium, aluminium, silicon and titanium are higher. The contents of chlorine and potassium are twice higher. Sodium and sulphur occur in small amounts at about 1%.

A relict of glaze slurry preserved in the glaze layer is characterised by a similar elemental composition as the glaze (Figure 7c,d and Table S2, RS). It contains, however, higher amounts of sodium (about 10–15%), aluminium, chlorine, titanium and iron. Small quantities of phosphorus and sulphur are also present. Additionally, Analysis No. 127 contains large amounts of barium at 25%. Small amounts of carbon in Analysis No. 133 correlate well with the qualitative analyses of the relicts of glaze slurry performed in low vacuum settings (see Table S1).

A colourant relict filling the hollow in the glaze is composed in almost 50% of iron (Figure S6d, RC). Additionally, it contains cobalt and carbon (10% each), zinc (6%), copper (about 4%) and aluminium (2.5%). Magnesium, titanium and silicon occur subordinately.

The main elements comprising the SSA structures include lead, calcium and phosphorus in variable proportions. Usually, they do not contain silicon and aluminium or these elements occur in trace quantities. Only Analysis Nos. 29 and 82 show the presence of silicon at about 10–15%. Chlorine at 1–3% occurs in all analyses. Trace quantities of magnesium, iron and copper occur in most of them. Single analyses contain trace quantities of sodium, potassium, chromium, titanium, strontium,

manganese, cobalt, nickel or arsenic. Additionally, Analysis No. 116 contains carbon. The structures are characterised by a low content of oxygen, usually not exceeding 10%.

The alloy infilling canaliculi (ALY) in the glaze has a similar chemical composition as the SSA (Table S2). It primarily contains lead (almost 50%), as well as calcium (about 20%). Phosphorus and silicon contribute to about 8%, and chlorine to 2%. The alloy comprises also sodium, potassium, copper, iron, aluminium and magnesium in quantities not exceeding 1%.

Interpretation

The presence of quartz grains in the upper part of the glaze layer indicates their detachment from the body layer during application of the glaze slurry. The grains must have been poorly bounded, which caused loosening of the bonds at the contact with the fluid slurry. This points to the application method during glazing and, at the same time, to single firing after forming the body and applying the glaze slurry on its surface. An additional argument testifying for a single firing is the fact of partial penetration of the glaze slurry into the body layer. If biscuit firing would have been applied, the glaze slurry could not have penetrated the body during glazing because the vitrified surface would have sealed the body interior, particularly its surface. The lack of a vitrified surface blocking the entry of the glaze slurry to the body interior caused its partial penetration. The glaze slurry was probably applied and distributed with a paintbrush, which additionally disrupted the grains on the body surface. During the firing process, the glaze slurry was characterised by mean viscosity and surface tension values, which points to a more fluid consistency. This is confirmed by the chemical composition of the glaze, dominated by elements decreasing viscosity. Such properties caused even distribution of the glaze slurry on the bowl walls and lack of stains.

Pores of variable sizes observed within the glaze layer are imprisoned gas bubbles. This fact may point to the melting and formation of soft glaze at an early firing phase, when processes of gas burning and release in the body layer were not finished yet. An additional factor favouring the formation of bubbles in the glaze is the high content of phosphorus derived from bone ash. Bubble formation in the glaze slurry and their behaviour after hardening of the glaze was possible due to moderate viscosity resulting from equivalent contents of aluminium and titanium, which increase viscosity, as well as magnesium, calcium, lead, sodium and potassium, which increase liquidity. This condition was sustained by the moderate surface tension of the glaze slurry, resulting from the similar content of elements increasing (Al, Mg, Ca) and decreasing (Ti, Pb, Na, K) its value [46].

Oval concentrations observed on the glaze and body contact were formed during melting of the glaze slurry. As a result of melting, its components including heavy elements formed oval concentrations, which were unreacted and sank in the fluid glaze alloy finally to set on the body grains. The concentrations increased their volume because of the rising temperature and additionally expanded the glaze. The resulting canaliculi were filled with alloy excess. The oval concentrations were solidified after firing and became cracked following thermal shrinkage during cooling. Structures occurring within the concentrations were formed during alloy crystallisation. Alloys may be good indicators of the firing temperature and require detailed investigations. The oval concentrations point to the excess of heavy components in some parts of the glaze. This results from the uneven distribution of glaze slurry on the body surface, which is linked not only with a nonuniform application of the mixture but also differences in the specific weight of the slurry components. Heavier fractions moved faster in the applied layer of glaze slurry and were set on the body grains.

Oval voids partly filled with alloy point to more advanced reactions with the glaze alloy. Most of the metal components in the alloy reacted forming the glaze. Only the relict alloy was retained in the oval voids.

The large oval hollow partly filled with glaze is the relict of a lower fragment of an air bubble (Figure S6c,d). The upper part of the bubble and the glaze layer are not preserved. This is indicated by the smooth surface of the rounded fragment of the glaze. The compressed air bubble developed close to the vessel wall during bowl moulding. Such bubbles, well-preserved as pores with smooth walls, are common in the body layer interior. Air accumulated in flattened bubbles close to the vessel surface

point to the compression mode of bowl moulding. The phenomenon could occur particularly in the lower mould when the air could not escape under the overburden of the upper mould. Being very thin, the roof of the bubble was destroyed during removal of the upper mould or during application of glaze slurry on the vessel surface. Slurry only partly infilled the developing hollow, whereas air formed the bubble. During firing, after glaze fluidisation, large bubbles burst on the surface, forming spherical hollows on the glaze surface. Cylindrical canaliculi developed when gaseous and liquid firing products migrated from the body and the IAL to the bowl exterior and their arrangement results from the stress pattern in the fluid (high viscosity) cooling glaze within the oval hollow. The cracks were formed during thermal shrinkage of the cooled down (stiff) glaze, and their pattern similar to the canaliculi is related to the coshaped extension of the still cooling alloy of the glaze. Relicts of material in variable forms in the large pore may be the remains of almost intact glaze slurry. The relicts could have entered the pore during drying of the slurry and become preserved in the air bubble. Large accumulation of the glass phase on the right side results from gravitational flow linked with the position of the vessel during firing.

The presence of lead in the glaze (GLZ, SSA, ALY) results from its usage as a flux. The use of lead also improved the optical brilliance of the glaze and decreased its viscosity during firing. Antimony as an accessory element in galena infrequently accompanies lead in the analyses. Calcium is a significant component of the glaze. Its addition was aimed at lowering the melting temperature of the glaze slurry and decreasing the viscosity of the glaze alloy in high temperatures, but also increasing the chemical durability after firing, which allowed for the usage of faience objects in contact with fluids. Large amounts of phosphorus in structures containing calcium and lead may point to the application of burnt bones, which were the sources of calcium and phosphorus. Copper and iron compounds were used for glaze colouring. The presence of both cupric and ferric ions might have resulted in the greenish-blue colour of the glaze. Besides giving the glaze a blue hue, copper in the content of about 2% played also the role of a strong flux that increased glaze liquidity, and enhanced solubility of lead in contact of the glaze with acids [47] (Table S2). Analysis of the relicts of glaze slurry indicates that beside quartz and colourant it also contained clay minerals, e.g., from the silty clay sediments of the Nile River, which is confirmed by the titanium or barium content in the glaze [48]. The lack of sulphur in the glaze results from its thermal decomposition in much lower temperatures than the firing temperature. Partly released sulphur was absorbed by clay minerals in the RS. An organic binder was also added to the glaze slurry, as indicated by the presence of carbon in the EDS and EGA analyses (Tables S1 and S2, see also Section 4.7). The alloy fragment with cobalt found in the glaze is not its colourant or maybe its content is too small to be detected by EDS analysis. It cannot be excluded that cobalt was used as a colourant for filling the relief and its fragment occurs in the glaze filling the hollow as a production impurity or fragment of relief paste that was introduced to the glaze slurry during application. Therefore, detailed studies of the relief components in the bowl should be performed. Analysis No. 1 has indicated that the canaliculi with darker edges occurring within the glaze (Figure S6a,b) are characterised by a similar composition as IPG in IAL. Explaining the similarities in the composition would require detailed microstructural analysis of the canaliculi and indicating their role during the firing process.

Interaction Layer

The body layer, comprising tightly packed quartz grains with a matrix composed of a glass phase (dark grey) occurs below the glaze layer. The matrix is not continuous and more or less tightly fills the voids between grains. The edges and corners of grains at the contact with the glass matrix are sharp (Figure S6a,b). The thickness of this layer varies from 50 to 100 μm . This is the layer of mutual impact (interaction) of the glaze and body (interaction layer (IAL)). Cracked quartz grains occur in the IAL and directly below in the body layer (Figure 7a and Figure S6a). The lower part of IAL is rough and in some places its boundary is blurry. Below occurs the body layer free of the glass matrix. Quartz grains in the body layer and rarely in the IAL are connected by interparticle glass (Figure 7b,c

and Figure S6b–d, IPG). Alloys (ALY) with irregular shapes occur below the IAL layer (Figure S6b). Analyses Nos. 31 and 33 resemble thermal degradation of mineral grains rather than spherical alloys as in the case of GLZ alloys (Table S2 and Figure S6b).

Interparticle glass (IPG) at the glaze and body contact (Figure 7c and Figure S6a,b,d) is composed mainly of silicon, potassium and aluminium. It also contains some calcium, iron, sodium and chlorine. Admixtures of titanium and sulphur occur in most analyses. Magnesium and phosphorus are present in a few analyses.

Alloys in the IAL have a different composition than alloys in the glaze (Fe-O, PX; Figure S6b, Table S2). Analysis No. 31 indicates an almost pure iron oxide. Aluminium, silicon, sulphur, potassium, calcium, titanium and vanadium occur in trace amounts. In Analysis No. 33 the content of iron and silicon is similar and reaches 20–30%. Alkali elements reach up to 3%. The content of calcium is only about 10%, and of aluminium, 6%. The partially melted grain also contains small amounts of titanium and manganese. Contrary to the glaze alloys, it does not contain phosphorus and lead, and the calcium content is much lower.

Interpretation

The upper part of the body layer with the glass matrix between the grains indicates an additional process of vessel surface preparation prior to the glaze slurry application. The increased content of such elements as sodium and potassium in the interparticle glass compared to the glaze layer indicates that the body surface could have been coated with a mixture containing these components, e.g., solution of a potassium/sodium salt and/or plant ash. During firing, a glass layer developed on the surface of the body layer below the forming glaze layer, which hampered the migration of fluid glaze that could penetrate the porous body structure. Melting of the applied glaze slurry as well the development of the glass phase could take place during firing due to melting of the body grains in reaction with salts or ash. Grain melting is not as intensive as in the glaze which contains large amounts of fluxes. The glass layer did not permit the penetration of fluid glaze into the body layer. After solidifying, the glass layer formed the glass matrix of the IAL, as evidenced by melted edges and corners of quartz grains in IAL and increased values of alkaline elements. The lack of such a glass phase protection layer could have caused complete penetration of the melting glaze into the porous body, resulting in a rough surface of the bowl with jutting out body grains. This is another argument for a single firing stage, during which a glaze layer and IAL with a glass matrix could be formed. The glass phase in IAL has similar properties as the glaze layer; a higher surface tension and lower viscosity in comparison to the IPG in the body layer. However, lack of copper in the IAL in relation to its presence in the glaze favoured the development of crazing on the glaze layer surface.

Irregular concentrations occurring at the IAL and body contact are relicts of alloys of heavy elements, which did not react and sank to this level. Due to the low content of heavy components in the applied glaze slurry, in some places, most of the alloy reacted and did not form oval concentrations. Their chemical composition indicates that Analysis No. 31 may represent the thermal transformation of magnetite to hematite and Analysis No. 33 partially melted iron and calcium aluminosilicate, e.g., pyroxene, most probably augite (compare Section 5.2).

The glass phase in IAL and the glaze alloy differ in chemical composition and properties. The glaze alloy is heavier but has a higher temperature being heated from the exterior and thus is thinner. The glass phase in IAL is lighter, but has a lower temperature due to cooling compared to the porous body and is denser. Therefore, the glaze alloy is active in relation to the glass phase from the IAL, mixing and reacting with it. Heavy element alloys concentrated on the glaze and IAL contact enhanced the reaction forming a glaze with a slightly lighter tint resulting from the increased content of these elements. After the firing process, the quick cooldown of the exterior glaze layer took place, which increased its density. At the same time, the glass phase in the IAL retained a higher temperature and was less dense. Differences in the chemical composition of the glass phase in the IAL compared to the glaze point to the relatively higher thermal expansion of the interaction layer, which favoured crazing. Therefore, during IAL cooling, tension stresses caused canaliculi formation, which developed from the glaze base

to its surface. The hampered possibility of fracture propagation to the surface due to the densifying glaze slurry induced the formation of horizontal canaliculi (Figure S6c).

Body Layer

The body layer continues below the interaction layer (IAL). At low magnification (several to over ten times) the layer is almost homogenous with only some exceptions (Figures 3–5, Figures S2 and S3). Larger differences can be viewed at a microscale. The basic components of the body layer are quartz grains of different sizes (Figures 7a and 8 and Figure S7, dark grey). The fraction below 50 μm (0.05 mm) is dominated by grains in the range of 10–20 μm (0.01–0.02 mm). A finer fraction is also present, from below 10 to about 2 μm . The body layer is slightly dominated by grains with diameters from 50 to 200 μm (0.05–0.2 mm). Additionally, single grains with higher dimensions of 200 to 500 μm (0.5 mm) occur. Such grain size distribution classifies the material as moderately sorted. Numerous grains are strongly cracked, particularly larger grains in the range of 100–200 μm (Figure S7a). Single grains of medium size, which underwent in situ disintegration into many smaller grains, have also been noted.

The quartz grains attain very diverse shapes in each of the distinguished fractions, from isometric through anisometric to elongated. The grains have sharp and jagged corners and edges. Irregular shapes resembling splinters or needles also occur. The grains are mainly angular and very angular. Elongated and anisometric, and low spherical grains prevail, whereas rounded grains are almost lacking. There is a very distinct orientation of elongated and anisometric grains (Figure 8a and Figure S7c). The best oriented are the largest and medium grains, whereas fractions below 30 μm are typically isometric and without any clear orientation. They mainly infill the voids between larger grains.

Evenly distributed aggregates of various sizes and irregular shapes occur between the grains in the entire body layer (Figure 8 and Figure S7, white areas). In some places, the aggregates are larger and reach maximally 80 μm . However, the largest number of aggregates occurs on the surface in the corners of quartz grains; their dimensions do not exceed 5 μm . In places where these aggregates are present, the glass phase as IPG (dark grey) creates connections between the grains. In the case of very small aggregates on grains, their surface is arch-like bent inwards.

Porous isometric aggregates occur also in the body layer (Figure 8a and Figure S7a, dark grey areas). Their sizes do not exceed 80 μm and they are irregularly distributed. The porous structure of these aggregates comprises a large number of bubbles of different sizes (10–20 μm), with very fine grains (1–2 μm) in the glass phase. The body also contains single mineral grains with authigenic shapes (Figure 8b–d). One grain is surrounded by a substance resembling the primary fragment of the mixture added to the silica paste.

The pore space is composed of pores of different sizes and shapes. Porosity between the grains comprises a large number of pores below 10 μm , which were formed between finer grains filling the space between medium grains (Figure 8c). Their shape is variable and depends on the grain shapes. The body layer also contains larger isometric pores, 50 to 200 μm in size. Some of them are oval or sub-oval, and some have jagged edges. The variable degree of packing of the grains in the body can be observed (Figures 7a and 8a, Figures S3 and S7a). Some zones with loose packing occur directly below the glaze and some within the body.

Quartz grains display enrichment in small amounts of iron, phosphorus and calcium, and trace amounts of titanium, chlorine, potassium, aluminium and sodium (Figure 7b and Table S2). Some of them are characterised by an almost 20% carbon content and 1% mercury content. The body layer contains plates of clay minerals and structures typical of these minerals (Figure 6a,b). Their presence was confirmed by the results of qualitative analyses (Table S1). Quantitative analyses of clay minerals observed in the thin section have indicated that they represent iron, titanium, potassium, magnesium and sodium aluminosilicates. Small amounts of potassium and lead in Analysis No. 45 may result from the impact of the alloy on the mineral grain (Figure 6b). Beside clay minerals, single grains of minerals that were not transformed during firing are observed in the body layer. They most probably include zircon (Zr) and ilmenite, an iron and titanium mineral (Fe-Ti; Figure 8c,d). Single grains with

lighter hues of grey than quartz and different shape. Their chemical composition is dominated by silicon. There is also sodium, potassium and aluminium.

Interparticle glass (IPG) from the body layer is characterised by a much narrower range of elemental composition compared to interparticle glass from the interaction layer (IPG). Beside silica it, contains about 8% aluminium, 4.5% potassium and below 1% iron.

The body layer does not contain spheroidal alloys as the glaze layer (Figure 8a,c and Figure S7b, ALY). Alloy aggregates are widely dispersed between the quartz grains. They are characterised by a wider range of chemical compositions (Table S2). All contain silicon and iron. The content of silicon is from 10 to almost 30%. However, Analysis No. 38 contains over 60% of silicon. In most analyses, the content of iron is 3–4%, with only 13% in Analysis No. 28. Almost all alloys contain significant contents of lead, and part of them also include antimony. Over half of the analyses occurs calcium at about 15%, and in Analysis No. 27 the content of this element is over 30%. Large contents of calcium are accompanied by large amounts of phosphorus. The contribution of the remaining alkali elements is low, with the highest values in Analysis No. 28. Alloys containing antimony do not contain chlorine. Contrary to the glaze alloys (ALY, SSA), they usually lack copper or contain only its trace quantities. Analyses with copper have also trace quantities of titanium.

Interpretation

The presence of quartz grains of various sizes from very fine to medium points to a precise and intentional mixture preparation as the main component of the silica paste. The quartz material was crushed to an expected fraction. Only single larger grains being manufacturing contaminations have been noted. Grain sieving in order to separate the nonfragmented grains into the expected fraction cannot be excluded. Many grains with anisometric shapes may indicate the fragmenting method and the applied tools. Cracks on grains, particularly the larger ones, resulted from intense crushing of the quartz material by pounding. The applied raw material could also possess acquired cracks which aided in the fragmentation process. Some cracks become apparent during the firing process, when expansion after heating and shrinkage after cooling took place. The large variability of the grain sizes and their high disintegration caused that after densifying the material became well packed, which significantly influenced the hardness and durability of the faience item. Proper preparation of the raw quartz material must have been well considered in order to achieve the highest possible packing of the silica paste during moulding of the faience object.

An almost complete lack of rounded grains as whole grains or their fragments indicates that the raw material used for the preparation of the basic silica paste component could not have been sand e.g., of aeolian origin. After fragmentation, such sand should bear traces of rounded surfaces and contaminants from the surface. Single grains with rounded surfaces are noted in the body, but they may represent only manufacturing contaminants, e.g., from other materials. Polycrystalline grains have not been observed, which excludes the usage of quartzose sedimentary or metamorphic rocks (sandstones or quartzites) as the raw material.

The in situ disintegration of larger grains, which resulted in very fine grains, below 10 μm in size, is commonly observed. Thermal transformations taking place on the surfaces of larger grains in the presence of fluxes caused granular disintegration. Fast heating of fluxes located between the grains caused heating of the surface zone and flaking of the finer fragments. The impact of fluxes is also observed on large grains (about 100 μm), which crack and disperse into many finer grains (Figure S7b–d). Hidden cracks formed during crushing could enhance the thermal disintegration of the grains. The other factors responsible are thermal expansion of minerals and α to β quartz transition [49]. Observations of the partially melted edges of quartz grains together with chemical composition analyses, clearly indicate high-temperature corrosion of quartz grains in a gaseous environment. Corrosion processes are controlled by the emission of gaseous particles from quartz material and strongly depend on the gas condition of the body-glaze system [50].

The common presence of irregular aggregates between the grains is the relicts of fluxes. The flux dispersed in the body layer caused the development of interparticle glass (IPG). Small,

several micrometres in size, glass bridges bound the quartz grains in one resistant skeleton and created a durable vessel (Figures 5d and 8c,d and Figure S7d). The number of such aggregates must have been larger, but glass bonds were formed due to melting. After firing arch-like hollows were created on the grain surfaces in places of flux aggregates.

Isometric aggregates (Figure 8a and Figure S7a, dark grey) are similar to the glass phase and their porous structure resembles a foamed glass mass. Very fine grains occurring within the glass phase are similar to quartz grains. These aggregates are relicts after intense sintering during the firing process in the presence of flux. Next, sintering of the powdered material concentrated between the grains took place. The alloy was formed mainly from metal grains, which played the role of flux, quartz grains and other admixtures. The isometric form of the aggregates indicates the concentration of the moist powder during the moulding of the silica paste. The powdered material required a much lower temperature from the melting temperature of particular components to achieve binding, melting and boiling. Some aggregates contain larger voids and the material is completely melted and homogenous. Glass slag aggregates with variable form and size, which depends on the initial composition of the mixture, were formed.

The presence of lead in the body also results from using it as a flux. Its coexistence with antimony in some analyses may indicate galena as the source of lead. Antimony as an accessory element may occur in variable amounts in galena. Some of the lead and antimony-containing structures seem to be crystalline phases. This may indicate the presence of synthetic bindheimite.

The body is composed mainly of quartz grains and admixtures, whose role was to maintain the shape of the vessel after moulding and to develop durable bonds between the grains after firing. Quartz, which is characterised by a very high coefficient of thermal expansion, should have caused strong thermal expansion during the firing process. The chemical composition of the developed bonds is similar to the composition of the glaze and glass phase in the IAL, which resulted in a similar coefficient of thermal expansion. Application of an admixture of clay minerals containing Al_2O_3 decreased expansion on the bonds. Additionally, the bonds did not form a continuous layer as the glaze, therefore their influence on the expansion of the body layer was insignificant. The value of the thermal expansion of the body layer must have exceeded the expansion of the IAL and the glaze layer. However, the body layer was not subject to significant expansion during firing because fluid IPG on the particle bonds allowed for microdisplacements in the pore space of the body. Large compression stress should have developed in the glaze layer during cooling due to the strong contraction of the body layer, but the observed case is just the opposite. Crazing is noted on the surface of the glaze layer due to tension stresses that developed as a result of larger thermal shrinkage of this layer in relation to the body layer. This situation may be explained by bonds formed between the quartz particles. During cooling, the bonds stiffened the skeleton of the body layer, which contradicted the thermal shrinkage of the body layer. The developing contraction stresses in the quartz crystals caused cracking of the grains. Therefore, a large number of cracked grains can be observed, especially in the contact zone of the body layer with the IAL. The developing cracks levelled the high thermal shrinkage of the body grain skeleton.

The authigenic shapes of different mineral grains, e.g., feldspars (albite and microcline), zircon and biotite, and admixtures to the silica paste point to the origin of raw material used to prepare the silica paste as the silty clay sediments of the Nile River and quartz veins from pegmatites. Contaminants derived from the applied stone tools used for disintegration of the raw material, which could have been made out of basalt, should not be excluded.

The orientation of the longer axes of elongated grains forming the vessel body parallel to the vessel walls could originate only during the moulding process. Longer grain axes were arranged perpendicularly to the largest pressure caused by stress. Such grain orientation points also to the silica paste consistency (firmness) during moulding. Oval and circular pores with smooth walls indicate the presence of air trapped in the silica paste during its formation. Uneven packing of the grains suggests the occurrence of variable amounts of fluid between the grains. Beside small amounts of

air, the entire pore space between the grains was filled with fluid—a mixture of water with mineral and organic binders—during the compression moulding of the silica paste. The variable content of fluid with a density exceeding water density caused loose packing of the grain skeleton. After firing the pore space between the grains remained empty, which resulted in high porosity confirmed by direct analyses (see Section 4.6). Grain orientation during the compression moulding was favoured by the fluid composed of water mixed with mineral and organic binders that occurred between the grains. Isometric pores with jagged edges were formed after the admixtures were completely or almost completely burnt out.

4.4. Image Analysis

Quantitative analysis allowed obtaining detailed characteristics of the grain skeleton and pore space parameters (Figure 9, Figure S8 and Table 1). The results of these analyses are presented below separately for both components of the faience body.

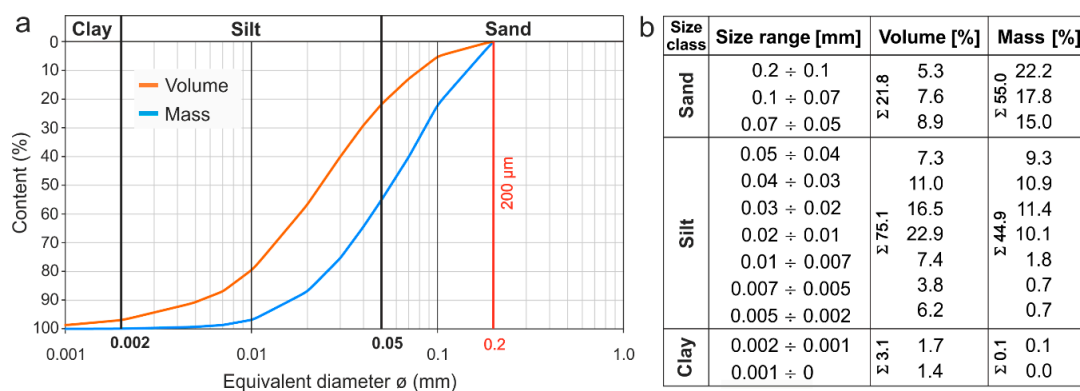


Figure 9. Quantitative characteristics of the grain skeleton in the faience body. (a) Grain size distribution curves. Note red line indicating 0.2 mm (200 μm) of equivalent diameter; (b) grain size composition.

Table 1. Quantitative characteristics of the faience body: morphometric and geometric parameters of the grain skeleton and pore space.

Grain Skeleton	Value	Pore Space	Value
Relative grains area s (%)	77.9	Porosity n (%)	31.4
Number of grains $N_s \times 10^3$	811	Number of pores $N_p \times 10^3$	154
Total area of grains $S_{st} \times 10^3$ (μm ²)	4051	Total area of pores $S_{pt} \times 10^3$ (μm ²)	1434
Average area of grains S_{sav} (μm ²)	9487	Average area of pores S_{pav} (μm ²)	9.3
Total perimeter of grains $P_{st} \times 10^3$ (μm)	4060	Total perimeter of pores $P_{pt} \times 10^3$ (μm)	1234
Average perimeter of grains P_{sav} (μm)	203	Average perimeter of pores P_{pav} (μm)	8
Average diameter of grains D_{sav} (μm)	5.5	Average diameter of pores D_{pav} (μm)	1.1
Sand $\varnothing > 50$ μm (%)	21.8	Mesopores $10 < \varnothing < 1000$ μm (%)	16.3
Silt $2 < \varnothing < 50$ μm (%)	75.1	Micropores $0.1 < \varnothing < 10$ μm (%)	83.7
Clay $\varnothing < 2$ μm (%)	3.1	Ultrapores $\varnothing < 0.1$ μm (%)	0
Average form index of grains K_{sfav} (-) *	0.421	Average form index of pores K_{pfav} (-) *	0.444
Isometric grains (%)	14.1	Isometric pores (%)	14.4
Anisometric grains (%)	79.8	Anisometric pores (%)	81.2
Elongated grains (%)	6.1	Fissure pores (%)	4.4

* parameter dimensionless.

4.4.1. Grain Skeleton

The values of parameters characterising the grain skeleton are presented in Table 1. The total grain area is 77.9%, at average grain area reaching almost 10,000 μm² (0.01 mm²). The average grain perimeter is 203 μm and the average grain diameter is 5.5 μm. Grain size distribution curves indicate

that the maximal grain diameter reaches up to 200 μm (0.2 mm). In the upper part, the curves are not bent asymptotically but reach the end of the chart in an almost straight line, whereas they are bent in the lower part of the chart and join tangentially (Figure 9). Grains with diameters from 200 to 50 μm and from 10 to 40 μm dominate, whereas grains below 10 μm are very rare. The mass curve is distinctly shifted with regard to the volume curve, which results from recalculating the grain size onto their mass. The largest differences occur for grains in the largest fractions, from 200 to 50 μm , which results from the fact that the volume of these grains is small but they constitute a large mass. On the histogram of the form index distribution, grains with anisometric and elongated shapes prevail, constituting 85.9% in total, whereas the remaining ones (14.1%) are isometric grains (Figure S8a).

Quantitative analysis of the fraction composition of the grain skeleton and the performed calculations have confirmed the qualitative observations (Figures 3–5, Figures 7 and 8, Figures S2, S3, S6, and S7). The matrix contributes to about 10% and the skeleton to about 65% of the volume. The remaining part is body porosity (Table 1). Precise fraction distribution and distribution of the content of the matrix particles are difficult to assess due to the fact that the matrix underwent the largest thermal transformations during firing. This accounts for a small error in the calculations, which may maximally reach 2–3%. The grain size distribution curve distinctly stops at a value of 0.2 mm.

4.4.2. Pore Space

The values of parameters characterising the pore space are presented in Table 1. Total porosity is 31.4% at an average pore area of about 10 μm^2 . Average pore perimeter is 8 μm , and average pore diameter is 1.1 μm . The histogram of the pore diameter distribution indicates that ultrapores are not present. Micropores dominate at 83.7%, and the remaining 16.3% represent mesopores (Figure S8c and Table 1). The maximal mesopore diameter reaches up to 137 μm . The detailed histogram of micropore distribution shows the lack of pores in the size range between 8.6 and 10.0 μm and a clear domination of pores between 0.1 and 1.7 μm (Figure S8d). The histogram of the distribution of the pore form index indicates the prevalence of anisometric and fissure pores, contributing to 85.6% in total, whereas the remaining 14.4% are isometric pores (Figure S8b). The rose of the orientation of the structural elements indicates that the anisotropy coefficient of the material building the faience body has an average value of 16.9%, which classifies the microstructure as medium oriented, and the preferred orientation direction of the structural elements is about 21° (see Section 5.1). Quantitative characteristics of the pore space also confirmed qualitative observations with regard to the occurrence of micropores as the main pore sizes in the faience body (Figure 5, Figure 7, Figure 8, Figures S6 and S7).

Interpretation

The absence of grains larger than 0.2 mm which indicates that precise sieving was applied (Figure 9a). Sieves were used after each stage of grinding to remove larger quartz grains that had not been entirely pulverised. This assured that larger grains were not used in subsequent manufacturing stages. The sieve mesh must have been about 0.2 mm, thus the quartz material being the base of the mixture used in subsequent manufacturing stages was perfectly prepared. During sieving, single larger grains could have passed through the mesh, but only those that were elongated, with the smaller dimension not exceeding the sieve mesh (Figure 8a).

The observed lack of micropores with sizes between 8.6 and 10.0 μm results from the low content of grains with diameters of 7 to 10 μm (Figure 9b and Figure S8). Rapid fall of the grain content below 10 μm may indicate the technical limits of the applied grinding tools. Anisometric and fissure pores are the most common, and analysis of the orientation of structural elements confirms the strongly oriented arrangement of the elongated grains (Figure S8a,b). These features again point to the strong compression of the silica paste during its moulding.

4.5. X-ray Powder Diffraction (XRD)

In the case of the samples studied, the most important test was the one that intended to verify the colourant present in the glaze on the outer surface of the bowl. Three diffraction graphs are presented in Figure S9, registering two different modes, i.e., the Bragg–Brentano method (MS-BDY_3h and MS-BDY_4h samples) and the DSH method (MS-GLZ_1h and MS-GLZ_3h samples). As seen in Figure S9a, quartz dominates in the samples. However, a closer look into the samples shows the presence of more phases, although their identification proved impossible for samples MS-BDY and MS-GLZ_1h. Cuprorivaite reflections can be seen in Figure S9b which is a scaled part of Figure S9a. This resulted in an increase in the absolute intensity of the reflections and in the emergence of a weak cuprorivaite reflection. Overall, the reflections are weak (Figure S9b), however they are strong enough to allow for phase identification. Longer duration of the body sample analysis (Figure S9c) allowed the detection not only quartz, but also small content of cristobalite, heat-treated sodium feldspar (albite) and potassium (microcline).

Interpretation

The main component of glaze is quartz. Among the strong reflections from quartz, reflections from cuprorivaite were registered, as well. The presence of cuprorivaite may be result of using it as a glaze colourant.

The dominant component of the body is quartz. Due to the strong reflections from quartz, weak reflections from cristobalite, plagioclase-albite and potassium feldspar-microcline were registered. The presence of feldspars as small impurities indicates that quartz veins from pegmatite rocks could be the source of raw quartz. Moreover, albite shows traces of high temperature treated during firing. Small amounts of cristobalite detected are probably the result of quartz exposure to high temperature and quick cooling after reaching the maximal firing temperature. The formation of this SiO₂ polymorph may take place at a temperature of about 900 °C [51].

4.6. Physical Properties

The specific density of the faience material is 2.84 Mg/m³ and its bulk density is 1.64 Mg/cm³. The calculated porosity value n is 42.4%, and the void ratio value e is 0.74. Porosity determined on the basis of image analysis is 31.4% (Table 1) and the calculated void ratio is 0.46.

Interpretation

The increased value of specific density in relation to the specific density of quartz (2.65 Mg/m³), which is the main component of this material, results from the presence of substances containing heavy elements, such as lead, iron, titanium or copper (see Tables S1 and S2).

The value of parameter n obtained from image analysis is understated by 11% in comparison to the calculated value. This results from the fact that the value obtained from image analysis refers to two dimensions of the sample (2D), whereas bulk density used for calculating parameter n was determined from a fragment of the faience bowl, i.e., using three dimensions (3D). Therefore, an error was created at anisotropy of the faience material, when the quartz grains are strongly elongated. Such error will not appear in the 2D analysis when the material will be isotropic [38]. The smallest pores related to the clay mineral content, which were not preserved during thin section preparation, were also excluded from the image analysis (see Figure 5).

The high value of porosity and low value of bulk density are related mainly to the quartz material defragmentation used for bowl manufacturing. Analysis of the grain size curve shows that the material is characterised by a high content of the silt and fine sand fraction (80%), and a small content of the very fine (10%; $\phi < 0.005$ mm) and coarse fractions (10%; $0.08 < \phi < 0.2$ mm; Figure 9). Such low variability of grain size coupled with the high content of grains of the silt fraction (75.1%) results in the high total porosity of the material. This results from the packing of the evenly grained material that lacks

additional fractions, particularly the fine ones, that would fill the pore space between the dominating grains. Large values of porosity result also from processes that took place during firing of the bowl. Part of the matter was completely burnt out and evaporated, and partly changed its form and structure. This is best visible in the voids between quartz grains where relicts of this matter can be observed. Surfaces, edges and corners of the quartz grains were subject to partial melting (see Figures 7 and 8, Figures S6 and S7). Defragmentation (crushing) of the quartz material took place not only during the preparation of the silica paste for moulding of the faience items. Cracking could be also caused by the high temperature during firing. This led to a slight increase in the pore space Figure S6a–d.

Based on studies of the physical parameters (bulk density and specific density) and calculations, only the general porosity value was obtained. Pore dimensions cannot be determined this way. SEM observations of the microstructure of the fracture surface have shown a large content of clay minerals in the material (Figure 5). Their content will increase the number of very small pores, i.e., ultra- and micropores (see Figure S8c,d and Table 1). However, SEM images of the thin sections did not display such high content of clay minerals. This is related to the removal of these smallest structural elements during thin section preparation. The lack of the finest fractions, whose contribution was not included in the quantitative image analysis, caused an error in the obtained content of the smallest pores (Figure 9).

4.7. Simultaneous Thermal Analysis (STA): TG-DSC with Evolved Gas Analysis (EGA): FTIR-QMS

The TG-DSC results obtained for the glaze and underglaze layer of the MS sample are presented in Figure S10a. They show that in the range of 35–1000 °C there was only a slight mass loss (about 5.2%) of the tested compound. Moreover, the mass loss took place in several stages. On the differential TG (DTG) curve two distinct endothermic peaks can be noticed, with maxima at 102 °C and 370 °C, respectively. The peak with a maximum of 102 °C, corresponding to 3.42% of mass loss, is probably related to the evaporation of the moisture contained in the sample. Analysis of the FTIR spectra (Figure S10b,c) indicates that water (absorption peaks at ~4000–3500 and 1800–1300 cm^{-1}) and carbon dioxide (absorption peaks at ~3800–3600, 2359–2310 and 669 cm^{-1}) were emitted while the sample was being heated. Water emission occurred from the beginning of the conducted study and the amount of water emitted increased gradually. In turn, the maximum carbon dioxide emission was observed at 380 °C. Taking into account the QMS results (Figure S10d), it can be supposed that at the beginning of heating, as the first evaporated the water present on the sample surface and then the water from inside the pores. Its decrease in the system was manifested by the decrease in the amount of the abundant ion m/z at 18. Initially, the amount of carbon dioxide evolved also decreased (decrease in the amount of abundant ion m/z at 44). However, at about 200 °C, a significant increase in its emission began and lasted till 380 °C, to decrease afterwards. A subsequent increase in CO_2 release is noted above 700 °C and continues until the end of the experiment at 1000 °C. This increase is not as rapid as previously. On the basis of FTIR spectra (Figure S10b) it can be assumed that during the heating of the sample, small amounts of ammonia were also emitted. This is indicated by the absorption peak at 3300 cm^{-1} . However, the presence of ammonia in the evolved gases is not confirmed by QMS measurements (lack of abundant ion m/z at 17), which may result from its very small amount.

Interpretation

The violent emission of CO_2 is related to the significant increase in gas volume in the oval pores of the glaze layer. The increase in gas pressure caused its pressing in the closed cracks, numerous in this layer (Figure 7 and Figures S4, S5a and S6). Pressure posed on the canaliculi walls and on pores caused cracking of the material and gas release. Two phases of carbon dioxide release point to a continuous process of gas adsorption by the glaze and pore formation during the firing. This results from an oxidising atmosphere that occurred in the kiln and from the stage-like firing of the organic binders. In turn, the release of small amounts of NH_3 may point to the use of an organic substance containing protein and/or a mineral constituent, e.g., ammonium salts. With regard to the DSC curve, it should be

noted that besides the endothermic peaks associated with gas emission, the endothermic peak with the maximum at 573 °C is also observed, which is associated with the transition of trigonal quartz (α -quartz) into hexagonal quartz (β -quartz; Figure S10a).

5. Reconstruction of the Moulding and Firing Processes

5.1. Moulding

Results of microscopic observations of the grain skeleton and pore space of the body layer were subject to analysis at three scales: (1) fragment of the fracture observed in an optical microscope, (2) entire surface of the thin section observed in a polarising microscope, and (3) fragment of the thin section observed in SEM (Figures 3c,d, 8a and 10, Figures S3 and S7a). Analysis of the entire surface of the thin section shows differences in the orientation of elongated grains. The parallel orientation of the longer axis of the grains with regard to the bowl walls is very distinct from the inside and in the middle part of the bowl cross-section, and very blurry on the outside and in the lower part of the bowl cross-section (Figure 10a). The orientation of the longer axis of oval pores is in accordance with the orientation of the longer axis of the grains (see also Figure S3b). Differences in packing have been noted, and the narrow and loose zones are in accordance with the orientation of the longer axis of grains and pores (Figures S3b and S7a). Observation in the optical microscope confirmed changes in the orientation of elongated grains in cross-section (Figures 3c,d and 10b). Analysis of SEM images has displayed a distinct orientation of elongate grains in the middle and on the bowl inside, as well as high anisotropy of the material (Figure S7a and Figure 10c,d). Anisometric and fissure pores as well as anisometric and elongated grains prevail in the body layer (Figure S8a,b and Table 1).

Based on the multiscale analysis of the grain skeleton and pore space of the body layer, the most probable technology of bowl moulding has been reconstructed. A two-part mould comprising an upper and lower part has been used for moulding (Figure 10e). The earlier prepared silica paste was uniformly distributed on the interior side of the lower part of the form. Next, the upper part of the form was inserted from above into the lower part and squeezed in order to achieve packing of the silica paste between the surfaces. During insertion of the upper form from above on the surface of the silica paste, small air bubbles were trapped in between. Voids surrounded by nonpermeable paste attained an oval shape during compression with a small slope of the longer axis. The continuing stress caused the reorientation of grains with their longer axes becoming perpendicular to the stress force. Free rotation and displacement of the grains was maintained by large porosity of the medium, the fluid mixed with mineral and organic binders, which infilled the pore space, and the fluid pressure in the pores. Due to the admixtures, the fluid had higher viscosity, which increased cohesion between the grains, decreased friction and enhanced plastic deformations of the silica paste. Differences in the orientation of elongated grains result from the distribution of stress which changed during moulding, along and across the silica paste layer (Figure 10f). Changes of the state of stress were related to the bowl shape. Distribution of normal and shear stress in the lower part, near the base, caused compression close to isometric and less distinct orientation of the elongated grains. In turn, the rounded part of the bowl was characterised by higher anisotropy of normal and shear stress, and the orientation of elongated grains is very clear. The increase in shear stress caused rotation of the elongated grains and orientation of their longer axes perpendicular to normal stress (Figure 10a,e,g). The increase in friction, the development of shear caused by the increase in shear stress, and the formation of narrow zones of low packed skeleton occurred during the insertion of the upper part of the form (compare Figure S3b with S7c). Distribution of stress in the bowl cross-section, particularly in the lower body with a convex wall, caused increased compression from the inside and extension from the outside, which resulted in local changes in the packing of the silica paste.

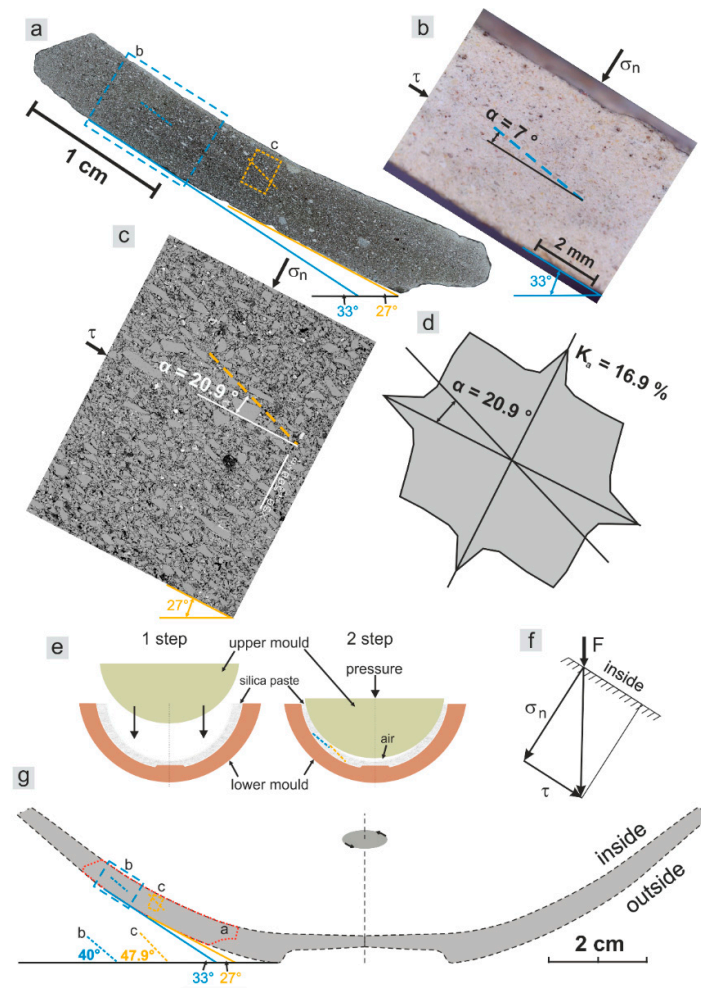


Figure 10. Moulding of the body layer examined by fresh fracture observation, thin section analyses and SEM study. (a) Large-format scan of the faience bowl: MS thin section (plane-polarised light, 1 nicol). The blue rectangle denotes the area enlarged in (b) and the orange rectangle denotes the area enlarged in (c). Note blue and orange dashed line and compare with the same dashed line in (g). The blue and orange lines with a number (in the lower part) indicate the angle of curvature of the bowl shape (compare with the same colour of line in (g)); (b) fragment of the area after cutting of bowl sample with the well-visible orientation of elongated grains in the body layer (light microscope). Note blue dashed line (orientation of elongated quartz grains) and compare with the same dashed line in (g,a). Blue angle with number (in the lower right side) indicates the curvature of the bowl shape; (c) SEM micrograph used in image analysis with the orientation of elongated grains (orange dashed lines). Image viewed in a high vacuum mode (HV) and backscattered electron mode (BSE) with $\times 50$ magnification. Orange angle with number (in the lower right side) indicates the curvature of the bowl shape; (d) rose of the orientation for structural elements in image (c). Compare orientation of elongated grains (marked with orange dashed lines in (c)) with the orientation from image analysis: rose of the orientation (α —direction of preferred orientation, K_a —anisotropy coefficient of the structural elements); (e) model of process moulding of the spherical bowl. Note blue and orange dashed line and compare with the same dashed line in (g,a); (f) state of stress in the body layer: F —pressure force, σ_n —normal stress, τ —shear stress; (g) cross-section through the spherical bowl (see reconstruction of shape in Figure 2b). The red dotted line indicates the area of the sample used for the preparation of the thin section, see (a). The blue rectangle denotes the area enlarged in (c) and orange rectangle denotes the area enlarged in (c); note blue and orange dashed line. The blue and orange lines with number (in the lower left side) indicate the angle of curvature of the bowl shape, and the blue and orange dashed lines with a number indicate the angle of orientation of elongated grains from (b,c).

After moulding, the porosity of the material was low. The pore space between the quartz grains was filled with various admixtures, such as fluxes, and mineral and organic binders. The silica paste was moist during moulding, so the material moulded by compression became more packed. This is evidenced by material anisotropy and distinct orientation of elongated quartz grains, which after compression became arranged with their longer axes perpendicular to the compressive stress. Binder addition enhanced such grain arrangement. Binders played the role of smear and allowed for shifting and rotation of grains, significantly decreasing friction between them. A small content of air was also present in the moist silica paste; during compression, it formed oval and slightly flattened bubbles (Figure 3b, Figure 4d, Figure 5a,b and Figure 7a, Figure S3b). The initial parameters of the material directly after moulding cannot be precisely determined. Obviously, the porosity value was much lower due to the presence of admixtures filling the pores between the grains. In turn, the parameters must have been sufficient enough for preserving the shape of the moist vessel after taking it out of the moulds and for bonding the skeleton grains by the added binders after drying. Therefore, the forces that caused packing of the material must have been large enough to meet these conditions. The material could slightly shrink and become more packed after drying, which influenced its hardness and durability, indispensable during later manufacturing stages.

5.2. Firing

Analysis of the results of multiproxy analyses allowed for precise determination of the temperature range, at which the bowl was fired (Figure 11). The following data were used: (1) crystalline phases in the body layer identified in the polarising microscope, (2) crystalline phases of the glaze and body layer identified in SEM with EDS, (3) microstructures and chemical composition of alloys in the glaze and body layer analysed in SEM with EDS, (4) XRD analysis of the glaze and body layer, and (5) DSC/TG with EGA and microstructure in SEM analysis of bubbles and gases in the glaze layer.

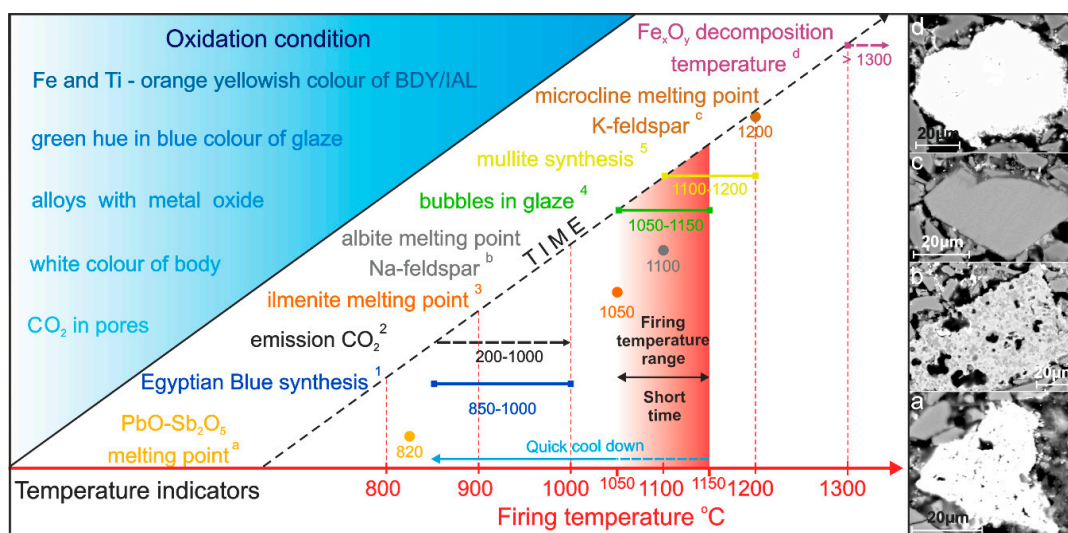


Figure 11. Firing of the faience spherical bowl examined by multiproxy data. Indexes a-d of temperature indicators correspond with images to the right: (a) synthetic equivalent of the mineral bindheimite (compare Figure S7b); (b) almost completely melted Na-feldspar (dark grey areas); (c) K-feldspar (intact structure); (d) iron oxide mineral: partly decomposed and oxidised magnetite. Indexes 1–4 of temperature indicators: ¹ synthetic mineral cuprorivaite (see Figure S9); ² increase emission of CO₂ trapped in the oval pores inside the glaze (see Figure S10b,c); ³ Fe-Ti mineral (see Figure 8d); ⁴ bubbles formation (see Figure 7c, Figures S4a and S6a,c,d); ⁵ sintering of clay mineral (see Figures 4 and 5).

Observations of biotite with a thermally strongly changed structure indicate temperatures exceeding 900 °C (Figure 8b, Table S2). Such values are confirmed by the Pb-Sb mixture which melted from a powdered metallic form (lead) or mineral (galena) and antimony (accessory element) at a temperature of at least 820 °C (Figure 11a) [52]. The reaction partially ended with the synthesis of bindheimite (Figure S7b and Table S2). The presence of this mineral is confirmed in the XRD analysis [3]. Small amounts of cuprorivaite crystals in the glaze layer indicate surpassing the temperature of 1000 °C (Figure S9b) [53]. Analysis of DSC/TG curves with EGA indicates that reactions in the sample did not terminate at 1000 °C, which means that the temperature of glaze firing must have been higher (Figure S10b–d). Observations of ilmenite, whose melting point is 1050 °C, have shown slight traces of melting, which indicate slight excess of this temperature level (Figure 8d and Table S2). Identification of Na-feldspar (albite) displaying strong traces of melting indicates that its melting point, 1100 °C was exceeded (Figure 11b) [54]. A large number of small bubbles (10–50 µm with the prevalence of sizes below 20 µm) in the glaze confirms a maximum firing temperature of 1050–1150 °C (Figure 7c, Figures S4a and S6a,c,d) [55]. Clay minerals were almost completely thermal transformed into other phases, and only in a few places single crystals were preserved, which means that the temperature between 1100 and 1200 °C was reached (Figures 4–6, Figure S5 and Tables S1 and S2). Additionally, the presence of partially melted pyroxene indicates temperatures below 1200 °C (Figure S6b, Analysis No. 33). The melting points of pyroxene minerals vary from 1200 to 1600 °C whereby the temperature decreases with increasing iron content [56]. Identification of K-feldspar (microcline melting point at 1200 °C (Figure 11c) [57]), iron oxide (decomposition temperature at least 1538 °C [58]), the almost intact structure of quartz and zircon grains without any modifications points to temperatures below 1200 °C. Microstructural observation of the magnetite grain surface may indicate its thermal transformation to hematite (Figure 11d) [59]. This confirms that the temperature of 1300 °C was not exceeded (Figure 8c,d and Table S2). Summarising, the firing temperature was most probably not lower than 1050 °C and not higher than 1150 °C. The temperature range was determined for crystalline phases from the glaze and body layer, which additionally points to a single firing stage.

Firing with a maximum temperature must have been very short because relicts of temperature indicators are preserved very well (Figure 11). Well-visible fluidal structures in the glaze, interaction layer and body, as well as the variety of forms and size of alloys, particularly the oval ones, point to rapid interruption of the firing process and quick cooldown in the high-temperature range (Figures 7 and 8, Figures S6 and S7). Only fine-crystalline mineral phases are preserved in some voids and circular pores left by alloys; they confirm the rapid termination of the firing process and quick cooldown (Figure 7c—middle-left part of the photograph and Figure S7d—lower left part of the photograph). A canaliculi and fracture network (crazing) developed within and on the surface of the glaze of a quickly cooled down item, which indicates a mismatch between the thermal expansion of the glaze with IAL and the body layer (Figure 7a and Figure S6b,c). Numerous pin-hole depressions in the glaze evidence a short high-temperature firing and thermal immaturity of the glaze (Figure 3e and Figure S4a). Detailed analysis of kilns and results of field studies from the Tell Atrib archaeological site should be performed to determine the total firing duration.

The studies enabled to reconstruct the conditions occurring in the kiln during the firing process (Figure 11). Application of cuprorivaite as the blue colourant, in which copper is oxidised at +2, in lead lustres gives a glaze colour with a green hue during firing in oxidised conditions. Emission of CO₂ already at 200 °C points to the beginning of the burning of the organic binder in oxidised conditions. Reduced conditions were not achieved during firing, as a result the body layer attains a white colour. The content of Fe and Ti gave the body a light orange hue at contact with the glaze due to firing in oxidised conditions. Alloys in the glaze and body layer form mixtures of Pb, Fe, Ti and Cu metal oxides with some alkali Ca, Al and Mg, as well as Cl and P. These facts point to the presence of oxidised conditions in the kiln throughout the firing process.

6. Discussion

So far, studies of faience objects were focused mainly on the analysis of the chemical composition of glaze in SEM integrated with EDS or WDS [14,60]. The lack of precise locality in the analyses does not allow for assessment and correct interpretations, as well as hampers precise comparisons. The results are not linked with SEM viewing of microstructures, whose diversity influences the chemical composition. As concluded from the performed analyses, detailed observations of microstructures coupled with precise localisation of chemical analyses have supplied novel and crucial information allowing for the reconstruction of the technologies used in faience manufacturing (see Section 4.3.3).

6.1. Raw Materials—Silica Paste

A dominating concept is that the source material for the quartz could have been ground quartz pebbles or quartz sand [1,12–14]. Our studies confirm that the silica paste was made out of quartz-rich rocks. The quartz material used for the preparation of the silica paste must have been homogenous because after firing the body layer is almost white and the only contaminants are relicts of the applied admixtures. The material was first crushed by pounding with a hard tool and then ground. The site has yielded numerous stone tools, including mortars and grinding pestles made out of hard rocks [61–63]. Therefore, the raw material must have been derived from rocks with pure quartz veins, e.g., magmatic rocks such as pegmatites. The source of the raw material could have been for example quartz-rich pebbles from gravels of the Edfu Formation, which are exposed in numerous localities along the Nile valley [64]. Lower Pleistocene gravels of this formation, rich in quartz pebbles of plutonic and quartz vein origin [65], are exposed close to the Tell Atrib site, about 75 km to the SSW in Saqqara around the Step Pyramid of Pharaoh Djoser. In turn, the usage of desert sand in the manufacturing of the studied hemispherical bowl should be excluded due to the lack of quartz grains with rounded edges, and a small amount of impurities, e.g., heavy minerals.

The large variability of the grain sizes and their high disintegration caused that after densifying the material became well packed, which significantly influenced the tightness and hardness of the faience item. Proper preparation of the raw quartz material must have been well considered in order to achieve the highest possible packing of the silica paste during the formation of the faience object. The use of rounded grains (sand) could have caused that the material would have been less cohesive during moulding and after drying of the bowl. In turn, angular material ensured better firmness.

6.2. Binders

The application of organic binders in faience manufacturing is still a matter of debate [5,13,14,18]. According to Vandiver [5], no macroscopic or chemical traces of the organic binder are left after firing. In turn, our studies have shown the presence of carbon in relicts of the glaze slurry, on the surfaces of quartz grains, and in C-Si ribbons formed during firing. Moreover, thermal analysis of the glaze has indicated the release of large amounts of carbon dioxide and small amounts of ammonia. The content of CO₂ in the glaze may be linked with the firing of organic matter. In turn, small amounts of NH₃ may come from the burning of protein from the organic binder or from the decomposition of salts containing ammonia. Shortland and Nicholson [14,18] proposed the addition of gum or resin as admixtures enhancing the moulding of vessels. Such admixtures will fulfil their function when added during paint production, but they will not achieve an adequate consistency of the silica paste for the moulding of vessels. The application of substances such as egg albumin or gelatine could have resulted in obtaining a fluid with an appropriate packing, and thus would result in an adequate consistency of the silica paste.

A controversial issue is the application of clay as an admixture for the silica paste. Nicholson [18] indicates several reasons why clay could not have been added at all or only sporadically to the silica paste. One of them is the fact that till Ptolemaic times, faience was produced without the addition of clay. The second reason is based on observations of fresh fractures of faience, which usually

have a white or grey tint and in macroscale bear no traces of clay addition. This must refer to the light-pink tint of the fracture, which is not observed in the studied fragment, and which should refer to the firing of clay to a light red colour. However, if e.g., kaolinitic clay would be added to the silica paste, then the fresh fracture of the faience body would maintain its white tint also after firing. An argument in favour for the addition of a small amount of clay material to the silica paste was the finding of numerous unfired clay vessels and kilns used for firing pottery and terra cotta in the Tell Atrib archaeological site [16,66–68]. The clay used for their manufacturing was subject to X-ray diffraction phase identification analysis. The mineral composition of the clay fraction was dominated by clay minerals such as illite, chlorite and kaolinite [68]. The presence of clay minerals was confirmed in numerous petrographic, microstructural and EDS analyses. The presence of partially thermal transformed clay minerals was confirmed in the matrix of the body layer. The existence of silica polymorph (cristobalite) which forms in high temperatures may indicate the initial stages of metakaolin and then mullite formation. Short high-temperature firing and a small amount of clay in silica paste influenced the limited possibility of their detection in XRD. It cannot be excluded that cristobalite may come either from quartz raw material or from Nile Delta silty clay sediments [69].

Application of organic binders and clay minerals resulted in larger packing of the silica paste and a high quality of the projected relief ornamentation. The applied reliefs with refined shapes inside and outside the bowl suggest that they could be formed simultaneously with moulding. Making the decoration after the moulding of a thin-walled vessel would have been a difficult and almost impossible task. Some decoration could have been added when the moulded bowl was still inserted in one of the forms. Therefore, the addition of components enhancing the plasticity of the silica paste was much wanted. After drying, the vessel maintained the desired shape and was not destroyed during glaze application. The organic binder was burnt out during firing, which increased the porosity of the body and at the same time decreased the weight of the vessel. Due to such high porosity, the faience object was much lighter from an analogous size item made of clay.

6.3. Moulding

Moulds were used in the manufacturing of faience vessels already from the fourth century BC, when the Macedonians arrived in Egypt [70]. However, it is not clear what they looked like and what they were made of. The moulds may have been analogous to those used in the production of clay bowls with relief decoration. It is also possible that clay vessels with relief decoration, like the ones found at Tell Atrib, may have been used as moulds for faience manufacturing [71]. Clay bowls with rim diameters from 13 cm to 20 cm, both plain and decorated with thin painted lines on the inside surfaces, resembled in shape and size faience bowls of B.1 type [3]. These bowls are dated between the mid-third century BC and the mid-second century BC, corresponding in date to the B.1 type bowl (Table S3). The dating is based on accompanying chronosensitive finds [29,31,32]. The correspondence may be more than accidental, suggesting that the potters making faience bowls may have patterned their products on clay counterparts, perhaps even using clay moulds for impressing the faience bowls. The decoration of both the faience and the clay bowls, especially the ones with relief decoration, demonstrates the mastery of local artisans employing different techniques to produce vessels in different materials. Fragments of gypsum moulds for the manufacturing of ceramics were discovered in Memphis. There is, however, no certain proof that such moulds were also used in the manufacturing of faience objects [18]. The performed studies show that the longer axes of elongated grains are oriented parallel to the vessel walls. This indicates that moulding of the bowl took place at intense compression in a two-part mould with an upper and lower part. Based on the regular shapes of faience objects from the Ptolemaic Period, Shortland [14] also suggest that vessel manufacturing must have taken place in moulds, but these authors link the two-part moulds with the manufacturing of very flat bowls or trays. In turn, deeper bowls, particularly those with deeply incised external decorations are typically associated with multipart moulds [14]. The application of multipart moulds is also indicated by ridges observed on the vessels in places where the moulds were connected with one another [72].

Welc and Nenna [3,13] discussed the uniqueness of decoration motives. Repeatability would have been large when the bowls would have been formed in moulds with a relief. The explanation to the low repeatability of decorations would have been the application of moulding forms to make the vessel and then using stamps to make the relief decorations. The observed repeatability of motives on the bowl decorations from Tell Atrib points to such technology of decoration. The use of stamps for the manufacturing of moulds for megarian bowls was suggested by Thompson [73]. However, obtaining convex reliefs inside the bowl using stamps is difficult to achieve. Additional microstructural and chemical composition analyses are required to determine the method used for decorating vessels with reliefs.

6.4. Glaze Slurry and Glazing

Ptolemaic faience belongs to one of the first cases of applying lead-alkali glaze in the antiquity [15]. The lead content in the glaze improved the optical brilliance and decreased its viscosity during firing [14,15,74]. The presence of lead in the glaze of the analysed bowl was confirmed by EDS analyses. Its concentrations in the form of spherical shaped alloys were noted at the glaze and IAL contact, as well as dispersed, irregular alloys of the body. Such large amounts of lead in the glaze and body layers indicate that Pb was also used as flux to drop the temperature in places where the alloy and glass were formed. This is confirmed by reactions observed in microstructures of the faience layered structure. Glaze rich in Al, Si, P, as well as Ca, Pb and Fe, points to the application of high firing temperatures to melt the components and produce high-fire glaze. Once again, this testifies for a single firing stage and high temperature of this process. Lead could have been added in metallic form as well as lead minerals, e.g., galena (lead sulphide (PbS)), as indicated by the presence of sulphur in the analyses. Despite the presence of lead antimonite (bindheimite) it should be excluded that this mineral was added on purpose. Bindheimite is very rare mineral but easy to synthesise. Small amounts of antimony present in galena could result in the synthesis of lead antimonite during firing of the faience bowl. The presence of lead objects, such as thin plates that were found during excavations may indicate that the processing of lead ores took place in Tell Atrib [75].

Addition of organic compounds and/or clay minerals allowed for obtaining a solution denser than water, which was indispensable for correct application of the glaze slurry on the faience item. In a water suspension, minerals containing heavy elements, e.g., galena, present in the mixture, will sink four times faster than the quartz grains of the same size. In turn, the addition of these compounds to the glaze slurry would cause even several tens slower sinking. Taking into account the thin layer of the glaze slurry applied on the surface, heavier grains could partly sink, therefore the alloy concentrations adjoin the body surface.

The small content of sodium in the glaze indicates that natron probably was not used for its production. Sodium may derive from plant ash or clay minerals in the glaze slurry. The high content of potassium and the presence of magnesium indicate the usage of plant ash, and the high content and proportion of calcium and phosphorus points to the addition of ashes from animal bones. The addition of calcium phosphate ($\text{Ca}_3(\text{PO}_4)_2$) from bone ash resulted in opaque glaze, as well as decreased the melting temperature of alloys in the glaze, IAL and body. The presence of calcium in glaze prevented its dissolution in water. A large number of bones (including burnt bones) found in Tell Atrib confirms that they must have been processed and used for different purposes, including the manufacturing of faience objects [75]. The high content of calcium could not come from the addition of grounded limestone. The firing of limestone would result in the emission of large amounts of CO_2 . This would cause a large number of bubbles in the glaze. The presence of chlorine both in the body and the glaze (Tables S1 and S2) may be related to the application of chlorides as fluxes in faience manufacturing.

Studies of Ptolemaic faience show that cobalt and copper compounds were applied as blue or green-blue colourants [14,15]. Our analyses have indicated the presence of copper in the blue-green glaze. The content of cobalt was confirmed by only one single grain (alloy?) in the glaze (Figure S6d and Table S2). Possibly, the total content of cobalt is insignificant so that it was not registered in the EDS

analysis, whereas detailed relief analyses may indicate its application. The source of the blue colourant is copper, perhaps in the form of synthetic mineral cuprorivaite (Egyptian Blue). The small amounts of Egyptian Blue detected in the XRD analysis, on the one hand, may be the proof for using cuprorivaite in faience making. On the other hand, its presence may be the result of the crystallisation of the cuprorivaite phase in glaze. Egyptian Blue could be manufactured in local workshops because its relicts have been found in the form of blue frit in the site; it was also discovered in painted plasters [28,76,77].

6.5. Firing

A so far unsolved issue is the number of firings of the faience items. Vandiver [1] assume the typical application of as a single firing. This was contested by Nicholson [18], who found fragments of fired and unglazed vessels from the Roman Period during the excavations at Memphis. He assumed that the body was biscuit fired at first at a higher temperature, and then with the applied glaze at a lower temperature. Our studies indicate that the application of mineral and organic binders and the appropriate preparation of the body surface before being covered by the glaze slurry allowed applying just a single firing. This conclusion is confirmed by numerous observations of the glaze and body microstructure coupled with analyses of the chemical composition. Two firing stages could be applied when a lower firing temperature was applied during biscuit firing. Such solutions were, however, not used in faience manufacturing. A second firing would have caused renewed melting of the grain bonds in the body layer and deformation of the item's shape. Therefore, biscuit firing did not have practical significance in this case. Detailed analysis of alloys composed mainly of Si, P, Ca and Pb, and their comparison with phase diagrams may confirm the temperature and number of firing stages. The double firing of faience is linked with the risk of damaging the item. The initially fired body contained interparticle glass (IPG) binding the quartz grains. In the subsequent firing, the temperature of the softening point for these bonds was lower than that required for the formation of these bonds. Exceeding this temperature during the second firing would have caused fluidisation of the bridges between the quartz grains and damage of the items during firing. Heaps of such damaged and melted vessels have been found in Memphis [18].

There are many factors considered to influence bubble formation in the glaze, among them is chemical composition. Bubbles in the lead glaze begin to form when the temperature exceeds 950 °C. The bubble number and size (30–80 µm) only slightly increase with temperature rise to 1150 °C. In turn, bubbles in the leadless glaze appear already at 850 °C, and their number and size (20–150 µm) significantly rise with temperature increase [55]. The presence of bubbles that are 10–50 µm in diameter, with the prevalence of sizes below 20 µm in the studied glaze point to a maximum firing temperature of 1050–1150 °C. A larger number of bubbles with smaller sizes may be caused by both lead and alkali content (Figure 7c, Figure S6a,c,d and Tables S1 and S2). Correlation between the firing temperature and the chemical composition of the glaze, in the relation to the formation of gas bubbles, confirms the use of calcium oxide (bone ash or burnt lime) instead of usage limestone.

6.6. Methodological Recommendations

Many interesting and important methodological comments regarding the multiproxy approach that emerged during the performance and development of research results have been included in File S1.

7. Conclusions

A multiproxy analysis of an ancient faience bowl performed in order to reconstruct ancient manufacturing technology has revealed the strengths and weaknesses of the investigative methods and their mutual dependence. Novel interpretation possibilities opened by the multiproxy approach have also led to significant conclusions regarding technological aspects of the manufacturing technology.

The silica paste was prepared from high-quality pure quartz extracted from veins of pegmatite origin, containing few impurities, e.g., feldspars and minerals rich in iron. The quartz raw material would have come from quarries or gravel sediments rich in quartz pebbles; the analysis excluded other rocks like sandstone, quartzite and sand. Clay minerals obtained from silty clay Nile sediments, a common raw material in the Athribian pottery and terracotta workshops, were also used for manufacturing faience.

Feldspars, clay minerals and bone ash were the sources of alkali fluxes (Na, K, Ca). Bone ash was also a source of calcium and phosphorus. Lead, which acted as a flux, was added in metallic or mineral form, e.g., as galena, a possibility indicated by a small amount of sulphur. Calcium present in bone ash acted as a stabiliser, increasing chemical resistance of the glaze to water. The source of chlorine, which is present in both body and glaze layer, remains unexplained.

Grinding quartz raw material with stone tools and sieving to select crushed material affected the shape and size of grains used for silica paste preparation. The plasticity of the paste was ensured by a small addition of mineral binder (clay minerals) and organic binder. Quartz grain selection and addition of binders resulted in good paste compaction during the moulding process and permitted thin-walled and richly decorated vessels to be produced. The clearly visible orientation of elongated quartz grains and the flattened pores in the body layer indicate moulding of the silica paste by compression in a multipart mould. The presence of binders ensured the durability of the form after drying and allowed for the application of glaze slurry without damaging vessel structure. This technique allowed for only one firing of the products. Use of organic binders is confirmed by large amounts of carbon absorbed into the quartz surface and the presence of gases: CO₂ and NH₃, in the pores of the glaze.

Relics of the glaze layer demonstrated that the slurry was a mix of finely ground quartz, clay minerals and bone ash with water added to allow application to the vessel surface. The colourant for blue-coloured glaze was copper, while small amounts of iron gave the glaze a greenish hue. The chemical composition of the glaze layer indicates cuprorivaite (Egyptian Blue) as a possible source of copper. The use of a metallic form of copper should not be excluded and the existence of Egyptian Blue crystals in the glaze may be related to their crystallisation during a rapid cooling process. The low content of alkali and the presence of iron and titanium are due to the raw materials used. Single quartz grains, detached from the body layer and embedded in the glaze layer, as well as the structural nature of the interaction layer between body and glaze indicate the use of a soft tool, e.g., a brush, for applying the glaze slurry. Appropriate proportioning of components of the slurry prevented the molten glaze from soaking too deeply into the body or running down the vessel walls during firing. Shrinking of the glaze upon cooling down was insignificant enough not to cause crazing.

The bowl was fired at a temperature of about 1050–1150 °C, in an oxidising atmosphere. Many indicators, e.g., geothermometers, that is, feldspars present in the body layer, and analysis of bubbles in the glaze layer gave a precise determination of the temperature, additionally confirmed by the observation of synthetic cristobalite, C-Si ribbons and partly melted quartz grain surfaces. The oxidising nature of the atmosphere in the kiln during firing was indicated by the presence of blue cupric ions and the identification of carbon dioxide from burning organic matter.

Applying such an advanced manufacturing technology gave a bowl of unusual aesthetic value, at the same time durable and much lighter than analogous pottery vessels. The use of copper and lead in the production process created a risk of heavy metal poisoning as a result of everyday use of the dishes.

The manufacturing methods involving preparation of the raw material and selection of admixtures at every stage of the process demonstrate technological knowledge and expertise drawing on the achievement of various craft workshops, such as pottery makers and metallurgical and casting ateliers. Therefore, faience items made in the Athribian workshops of Ptolemaic times are truly the first high-tech ceramics in the world.

Supplementary Materials: The following are available online at <http://www.mdpi.com/2075-163X/10/9/785/s1>, File S1: Methodological recommendations, Figure S1: Diagram of the multi-proxy analysis for MS samples, Figure S2: Fragments of the layered structure of the faience bowl observed under digital and stereoscopic light microscopy and prepared for microstructural investigations. (a) fragments of the glaze surface and glaze bottom are well-visible. White rectangles denote the area in Figure S4a,c; (b) well-visible relicts of silica paste, relicts of glaze slurry and C-Si ribbon. White rectangles denote the area in Figures S5d and 6a; (c) fragments of the body layer; (d) enlarged fragments of the layered structure from (a)–(c) are well-visible (arrowed). Note C-Si ribbons on the surface of glaze bottom (left fragment) and body (right fragment), Figure S3: Large-format scan of the faience bowl—MS thin section. Orientation of the images: T–B (B—right side, see Figure 2). (a) plane-polarised light (1 nicol). BDY—body layer, GLZ—glaze layer, IAL—interaction layer, loosely packed—enlarged area in Figure 7a, hollow—enlarged area in Figure S6c; (b) cross-polarised light (2 nicols). Loosely packed—similar area, see Figure S7a, Figure S4. Title and captions, see Figure 6. Colour number with a dot, oval or rectangle marks the localisation of the EDS analyses (see Table S1). (a) melted quartz grains (Q), spherical pores (SP), canaliculi (CL), cracks (CR), spherical shaped alloy (SSA) and alloy (ALY) well-visible within the glaze; (b) analyses located in image (a); (c) glaze and underglaze layer with well-visible melted quartz grains, spherical pores, alloys, spherical shaped alloys and relict of glaze slurry (RS); (d) analyses located in image (c). The white rectangle denotes the area enlarged in (e); (e) well-visible spherical shaped alloys, Figure S5: Title and captions, see Figure 6. Colour number with a dot or rectangle marks the localisation of the EDS analyses (see Table S1). (a) glaze and underglaze layer with melted quartz grains, spherical pores, alloys, spherical shaped alloys and relict of glaze slurry (RS); (b) nearly hemispherical relict of glaze slurry; (c) analyses located in image (b); (d) clod relict of glaze slurry; (e) analyses located in image (d), Figure S6: Title and captions, see Figure 7. (a) spherical alloys are visible between the glaze and underglaze layer (arrowed). A large number of canaliculi in the glaze (arrowed) and interparticle glass well-visible. Partially melted quartz grain sticking out above the glaze surface; (b) many spherical alloys are visible between the glaze and underglaze layer and in the interaction layer (arrowed). Many canaliculi and spherical pores are found in the glaze (arrowed); (c) interaction layer surrounding an oval hollow with glaze. Singular spherical alloy and spherical pore as well as cracks and canaliculi are visible (arrowed). The white rectangle denotes the area with hollow enlarged in (d); (d) fragment of hollow. Well-visible interaction between the glaze and interaction layer, Figure S7: Title and captions, see Figure 8. (a) fragment of the body with high orientation of elongated quartz grains. Large fissure pore space with the same orientation as the elongated grains is visible in the centre. Many fractured grains well-visible (arrowed); (b) synthetic bindheimite (BIN) surrounding melted grains of quartz (in the centre). Note grain of slag mixed with alloy (upper side); (c) high orientation of elongated quartz grains surrounding pore with alloys (in the centre, ALY). White rectangle denotes the area enlarged in (d); (d) alloy (ALY) surrounding fractured quartz grain, Figure S8: Quantitative characteristics of the grain skeleton and pore space in the faience body. Probability density of grains/pores $Ph_i = N_i/N \cdot l$: N_i —number of grains/pores within the “ i ” interval, N —total number of grains/pores, l —length of the interval. The distribution of the equivalent diameter (D) allowed determining micropore (0.1–10 μm) and mesopore (10–1000 μm) contents. Grains/pores with different shapes were distinguished based on the distribution of the form index (K_{sf}/K_{pf}): isometric $a/b < 1.5$, anisometric $1.5 < a/b < 10$ and elongated/fissure $a/b > 10$ (a , b —extreme grain/pore dimensions). (a) histogram of the form index of grains shape K_{sf} distribution; (b) histogram of the form index of pore shape K_{pf} distribution; (c) histogram of diameter D of meso- and micropore distribution; (d) histogram of diameter D of micropore distribution, Figure S9: X-ray Powder Diffraction Analysis (XRD) of the faience body and glaze and underglaze layer. (a) diffractograms of MS-BDY and MS-GLZ samples with symbols of reflections: Q—quartz, ?—reflection of phases, which could not be identified with certainty; (b) enlarged diffractograms of MS-BDY and MS-GLZ samples with symbols of reflections: Q—quartz, Cu—cuprorivaite, ?—reflection of phases, which could not be identified with certainty; (c) diffractogram of MS-BDY sample with symbols of reflections: Q—quartz, Cr—cristobalite, Pl—plagioclase, K—potassium feldspar, ?—reflection of phases, which could not be identified with certainty, Figure S10: Simultaneous Thermal Analysis—STA (DSC-TG) with Evolved Gas Analysis—EGA (QMS-FTIR) of the faience glaze and underglaze layer. (a) TG, DTG and DSC curves; (b) FTIR spectra of gaseous products evolved during thermal analysis for selected temperatures; (c) 3D diagrams of FTIR spectra of gaseous products evolved during thermal analysis; (d) QMS spectra for the ions of $m/z = 18$ and 44, Table S1: Elemental composition of the faience layered structure. Localisation and spectrum of EDS analyses, see Figure 6, Figures S4 and S5, Table S2: Elemental composition of the faience layered structure. Localisation of EDS analyses, see Figure 7, Figure 8, Figures S6 and S7, Table S3: The dating of clay bowls based on accompanying chrono-sensitive finds. Reference [78] is cited in the supplementary materials

Author Contributions: Conceptualization, J.T. and M.Z.; sample providing, F.W.; methodology, J.T., M.Z.; measurements, J.T., M.Z., M.R., G.K.; data analysis and interpretation, J.T., M.Z.; archaeological support, A.P., F.W.; writing—draft preparation, J.T., M.Z.; writing—review and editing, J.T., M.Z., M.R. and A.P. All authors have read and agreed to the published version of the manuscript.

Funding: This research was funded by the Polish National Science Centre, grant number 2017/27/N/HS3/02464.

Acknowledgments: We would like to offer our sincere gratitude to Professor Karol Myśliwiec, director of the Polish-Egyptian Archaeological Mission working in Tell Atrib in 1985–1995 under the auspices of the Polish Centre of Mediterranean Archaeology University of Warsaw, for his assistance in making this research possible. We would like to thank Marek Barański for consultation and discussion on the mechanical analysis of the moulding process, all the reviewers and the Editorial Board who were involved in the process of improving the manuscript and

preparing it for publication. All comments were very valuable and helped us to improve the content and visual aspect of the article.

Conflicts of Interest: The authors declare no conflict of interest. The funders had no role in the design of the study; in the collection, analyses, or interpretation of data; in the writing of the manuscript, or in the decision to publish the results.

References

1. Vandiver, P.B.; Kingery, W.D. Egyptian Faience, The First High-Tech Ceramic. In *Ceramics and Civilization III: High-Technology Ceramics. Past, Present and Future*; Kingery, W.D., Ed.; American Ceramics Society: Columbia, OH, USA, 1987; pp. 19–34.
2. Nicholson, P.T. *Egyptian Faience and Glass*; Shire Publications LTD.: Buckinghamshire, UK, 1993.
3. Welc, F. *IV Tell Atrib 1985–1995. Faience Objects*; University of Warsaw Press: Warsaw, Poland, 2014.
4. Kaczmarczyk, A.; Hedges, R.E.M. *Ancient Egyptian Faience: An Analytical Survey of Egyptian Faience from Predynastic to Roman Times*; Aris & Phillips: Warminster, UK, 1983.
5. Vandiver, P.B. Egyptian faience technology, Appendix A. In *Ancient Egyptian Faience*; Kaczmarczyk, A., Hedges, R.E.M., Eds.; Aris and Phillips: Warminster, UK, 1983; pp. A1–A144.
6. Tite, M.S.; Freestone, I.C.; Bimson, M. Egyptian faience: An investigation of the methods of production. *Archaeometry* **1983**, *25*, 17–27. [[CrossRef](#)]
7. Tite, M.S.; Bimson, M. Faience: An investigation of the microstructures associated with the different methods of glazing. *Archaeometry* **1986**, *28*, 69–78. [[CrossRef](#)]
8. Vandiver, P. Egyptian faience technology. In *Archaeological Ceramics*; Franklin, A.D., Olin, J.S., Eds.; Smithsonian Institution Press: Washington, DC, USA, 1982; pp. 167–179.
9. Tite, M.S.; Shortland, A.J.; Kaczmarczyk, A.; Vandiver, P. Faience production in Egypt. In *Production Technology of Faience and Related Early Vitreous Materials*; Shortland, A., Tite, M.S., Eds.; Oxford University School of Archaeology: Oxford, UK, 2008; pp. 57–91.
10. Matin, M.; Matin, M. Egyptian faience glazing by the cementation method part 1: An investigation of the glazing powder composition and glazing mechanism. *J. Archaeol. Sci.* **2012**, *39*, 763–776. [[CrossRef](#)]
11. Wulff, H.E. *The Traditional Crafts of Persia*, 1st ed.; MIT Press: Cambridge, UK, 1966.
12. Petrie, W.M.F. *Tell el Amarna*; Methuen & Co.: London, UK, 1894.
13. Nenna, M.D.; Seif el-Din, M. *La Vaissele en Faience d’Epoque Gréco-Romaine, Catalogue du Musée Gréco-Romain d’Alexandrie*; Institut Français d’Archéologie Orientale: Cairo, Egypt, 2000.
14. Shortland, A.J.; Tite, M.S. Technological study of Ptolemaic—Early roman faience from Memphis, Egypt. *Archaeometry* **2005**, *47*, 31–46. [[CrossRef](#)]
15. Mao, Y. Lead-Alkaline Glazed Egyptian Faience: Preliminary Technical Investigation of Ptolemaic Period Faience Vessels in the Collection of the Walters Art Gallery. *J. Am. Inst. Conserv.* **2000**, *39*, 185–204. [[CrossRef](#)]
16. Scholl, T.; Daszkiewicz, M.; Raabe, J. Kilns from the Ptolemaic Period in Tell Atrib. *Etudes Trav.* **1995**, *27*, 279–307.
17. Nicholson, P.T.; Jackson, C.M. Tell el-Amarna and the glassmakers’ workshop of the second millennium B.C. In *La Route Du Verre. Ateliers Primaires Et Secondaires Du Second Millenaire Av. J.-C. Au Moyen Age*; Nenna, M.-D., Ed.; Maison de l’Orient Méditerranéen: Lyon, France, 2000; pp. 11–20.
18. Nicholson, P.T. *Working in Memphis, The Production of Faience at Roman Period Kom Helul*; Egypt Exploration Society: London, UK, 2013.
19. Michałowski, K. Les fouilles polonaises à Tell Atrib (1957–1959). *Ann. Serv. Antiq. l’Égypte* **1962**, *57*, 49–66.
20. Kołodziejczyk, K. Report of the Polish Archaeological Mission’s Excavations at Tell Atrib in 1963. *Etudes Trav.* **1972**, *6*, 137–145.
21. Młynarczyk, J. Egyptian Types of Terracotta Lamps from Tell Atrib. *Etudes Trav.* **1973**, *7*, 81–113.
22. Ruszczyk, B. Tell Atrib. In *50 lat Polskich Wykopalisk w Egipcie i na Bliskim Wschodzie*; Kiss, Z., Ed.; Polish Centre of Mediterranean Archaeology: Warsaw, Poland, 1986; pp. 29–34.
23. Myśliwiec, K. Polish-Egyptian excavations at Tell Atrib in 1989. In *Polish Archaeology in the Mediterranean I Reports 1988–1989*; Koliński, R., Ed.; Polish Centre of Mediterranean Archaeology: Warsaw, Poland, 1990; Volume 1, pp. 5–9.

24. Myśliwiec, K. Polish-Egyptian excavations at Tell Atrib in 1990. In *Polish Archaeology in the Mediterranean II: Reports 1989–1990*; Gawlikowski, M., Daszewski, W.A., Eds.; Polish Centre of Mediterranean Archaeology: Warsaw, Poland, 1991; Volume 2, pp. 25–30.
25. Szymańska, H. Tell Atrib. Excavations, 1998. In *Polish Archaeology in the Mediterranean X: Reports 1998*; Gawlikowski, M., Daszewski, W.A., Eds.; Polish Centre of Mediterranean Archaeology: Warsaw, Poland, 1999; Volume 10, pp. 71–76.
26. Myśliwiec, K. In the Ptolemaic Workshops of Athribis. *Egypt. Archaeol.* **1996**, *9*, 34–36.
27. Myśliwiec, K. Rescue Excavations at Tell Atrib in 1985–1995. In *Tell Atrib 1985–1995 I*; Myśliwiec, K., Sztetyło, Z., Eds.; ZAŚ PAN & Neriton: Warsaw, Poland, 2000; pp. 13–68.
28. Myśliwiec, K. Contexte archeologique. In *Tell Atrib 1985–1995 II*; Myśliwiec, K., Krzyżanowska, A., Eds.; ZAŚ PAN & Neriton: Warsaw, Poland, 2009; pp. 9–49.
29. Młynarczyk, J. *Terracotta Oil Lamps. Tell Atrib 1985–1995 III*; IKŚiO & Neriton: Warsaw, Poland, 2012.
30. Welc, F. Faiences from Greco-Roman Athribis. Ph.D. Thesis, University of Warsaw, Warsaw, Poland, 2009.
31. Sztetyło, Z. Pottery stamps. In *Tell Atrib 1985–1995 I*; Myśliwiec, K., Sztetyło, Z., Eds.; ZAŚ PAN & Neriton: Warsaw, Poland, 2000; pp. 53–168.
32. Krzyżanowska, A. Les monnaies. In *Tell Atrib 1985–1995 II*; Myśliwiec, K., Krzyżanowska, A., Eds.; ZAŚ PAN & Neriton: Warsaw, Poland, 2009; pp. 75–204.
33. Myśliwiec, K. Polish-Egyptian excavations at Tell Atrib in 1994. In *Polish Archaeology in the Mediterranean VI: Reports 1994*; Gawlikowski, M., Daszewski, W.A., Eds.; Polish Centre of Mediterranean Archaeology: Warsaw, Poland, 1995; Volume 6, pp. 37–47.
34. Welc, F. Decorated Ptolemaic faience bowl from Athribis (Tell Atrib), Nile Delta. *Etudes Trav.* **2011**, *24*, 243–270.
35. Sergeyev, Y.M.; Spivak, G.V.; Sasov, A.Y.; Osipov, V.I.; Sokolov, V.N.; Rau, E.I. Quantitative morphological analysis in a SEM–microcomputer system–I. Quantitative shape analysis of single objects. *J. Microsc.* **1984**, *135*, 1–12. [[CrossRef](#)]
36. Sergeyev, Y.M.; Spivak, G.V.; Sasov, A.Y.; Osipov, V.I.; Sokolov, V.N.; Rau, E.I. Quantitative morphological analysis in a SEM–microcomputer system–II. Morphological analysis of complex SEM images. *J. Microsc.* **1984**, *135*, 13–24. [[CrossRef](#)]
37. Sokolov, V.N.; Yurkovets, D.I.; Razgulina, O.V. *Stiman (Structural Image Analysis): A Software for Quantitative Morphological Analysis of Structures by Their Images (User’s Manual. Version 2.0)*; Laboratory of Electron Microscopy, Moscow State University: Moscow, Russia, 2002.
38. Trzciniński, J. Combined SEM and computerized image analysis of clay soils microstructure: Technique & application. In *Advances in Geotechnical Engineering: The Skempton Conference, Proceedings of the Three Day Conference on Advances in Geotechnical Engineering, Royal Geographical Society, London, UK, 29–31 March 2004*; Jardine, R.J., Potts, D.M., Higgins, K.G., Eds.; Thomas Telford: London, UK, 2004; pp. 654–666.
39. Grabowska–Olszewska, B.; Osipov, V.I.; Sokolov, V.N. *Atlas of the Microstructure of Clay Soils*; Państwowe Wydawnictwo Naukowe: Warsaw, Poland, 1984.
40. Smart, P.; Tovey, K. *Electron Microscopy of Soils and Sediments: Techniques*; Oxford University Press: Oxford, UK, 1982.
41. Sokolov, V.N. Engineering–geological classification of clay microstructures. In *Proceedings of the 6th International Congress IAEG, Amsterdam, The Netherlands, 6–10 August 1990*; Price, D.G., Ed.; CRC Press: Cleveland, OH, USA, 1990; pp. 753–760.
42. *BS 1377-2: 1990 Methods of Test for Soils for Civil Engineering Purposes-Part 2: Classification Tests*; British Standards Institution: London, UK, 1990; pp. 26–27.
43. Simonis, H. Practical Suggestions for Control of Glaze Defects. Pt. 2. *Keram. Z.* **1980**, *32*, 593.
44. Taylor, J.R.; Bull, A.C. *Ceramics Glaze Technology*; Pergamon Press: Oxford, UK, 1986.
45. Zhang, H.; Ding, W.; He, K.; Li, M. Synthesis and Characterization of Crystalline Silicon Carbide Nanoribbons. *Nanoscale. Res. Lett.* **2010**, *5*, 1264–1271. [[CrossRef](#)] [[PubMed](#)]
46. Britt, J. *The Complete Guide to High-Fire Glazes*; Lark Books: New York, NY, USA, 2007.
47. Mohamed, N.; Chin, Y.M.; Pok, M.W. Leaching of lead from local ceramic tableware. *Food Chem.* **1995**, *54*, 245–249. [[CrossRef](#)]
48. Garzanti, E.; Andò, S.; Limonta, M.; Fielding, L.; Najman, Y. Diagenetic control on mineralogical suites in sand, silt, and mud (Cenozoic Nile Delta): Implications for provenance reconstructions. *Earth Sci. Rev.* **2018**, *185*, 122–139. [[CrossRef](#)]

49. Shen, Y.J.; Zhang, Y.L.; Gao, F.; Yang, G.S.; Lai, X.P. Influence of Temperature on the Microstructure Deterioration of Sandstone. *Energies* **2018**, *11*, 1753. [[CrossRef](#)]
50. Lai, G.Y. *High-Temperature Corrosion and Materials Applications*; ASM International: Materials Park, OH, USA, 2007.
51. Flörke, O.W.; Graetsch, H.; Jones, J.B. Hydrothermal deposition of cristobalite. *N. Jb. Miner. Mh.* **1990**, *2*, 81–95.
52. Levine, E.M.; Robbins, R.; McMurdie, H.F.; Reser, M.R. *Phase Diagrams for Ceramicists*; American Ceramic Society: Columbus, OH, USA, 1964.
53. Pradell, T.; Salvado, N.; Hatton, G.D.; Tite, M.S. Physical Processes Involved in Production of the Ancient Pigment, Egyptian Blue. *J. Am. Ceram. Soc.* **2006**, *89*, 1426–1431. [[CrossRef](#)]
54. Greenwood, J.P.; Hess, P.C. Congruent melting kinetics of albite: Theory and experiment. *J. Geophys. Res. Solid Earth* **1998**, *103*, 29815–29828. [[CrossRef](#)]
55. Xiong, L. Glaze Surface Tension Effects on Bubble Evolution. Master's Thesis, Alfred University, Alfred, NY, USA, 2004.
56. Kearey, P. *The Encyclopedia of the Solid Earth Sciences*, 2nd ed.; Wiley-Blackwell: Oxford, UK, 2009.
57. Fang, H.Y.; Chaney, R.C. *Introduction to Environmental Geotechnology*, 1st ed.; CRC Press: Boca Raton, FL, USA, 1997.
58. Samsonov, G.V. *The Oxide Handbook*, 2nd ed.; IFI/Plenum: New York, NY, USA, 1982.
59. Simmonds, T.E. The High Temperature Decomposition of Hematite under Reactive Gas Atmospheres: For the Use in Chemical Looping Combustion. Master's Thesis, The University of Queensland, St. Lucia, Australia, 2017.
60. Tite, M.S.; Panagiota, M.; Shortland, A.J. A technological study of ancient faience from Egypt. *J. Archaeol. Sci.* **2007**, *34*, 1568–1583. [[CrossRef](#)]
61. Ruszczyc, B. Tell Atrib Register of finds. Unpublished work, 1980.
62. Myśliwiec, K. Tell Atrib Register of finds. Unpublished work, 1985.
63. Myśliwiec, K. Tell Atrib Register of finds. Unpublished work, 1986.
64. Said, R. *The Geological Evolution of the River Nile*; Springer: New York, NY, USA, 1981.
65. Wysocka, A.; Welc, F.; Czarniecka, U. Sedimentary environment of the early Pleistocene gravels of the Edfu Formation from the Saqqara archaeological site (Egypt)—Preliminary results. *Studia Quat.* **2016**, *33*, 69–78. [[CrossRef](#)]
66. Myśliwiec, K. Polish-Egyptian Excavations at Tell Atrib in 1991–1993. *Etudes Trav.* **1995**, *17*, 205–239.
67. Myśliwiec, K.; Południkiewicz, A. A center of ceramic production in Ptolemaic Athribis. In *Egyptian Pottery, Proceedings of the 1990 Pottery Symposium at the University of California, University of California, Berkeley, NC, USA, 2003*; Redmount, C., Keller, C., Eds.; Regents of the University of California: Berkeley, NC, USA, 2003; pp. 133–152.
68. Południkiewicz, A. Unfired Pottery from Ceramic Workshops at Tell Atrib with Appendix by Daszkiewicz, M., Raabe, J., The Clay and Unfired Ceramic Fragments from Tell Atrib—Preliminary Report on Technological Investigations. In *Hellenistic and Roman Pottery in the Eastern Mediterranean—Advances in scientific studies, Acts of the II Nieborów Pottery Workshop, Nieborów, Poland, 18–20 December 1993*; Meyza, H., Młynarczyk, J., Eds.; ZAŚ PAN: Warsaw, Poland, 1995; pp. 299–329.
69. Jones, J.B.; Segnit, E.R. Genesis of cristobalite and tridymite at low temperatures. *J. Geol. Soc. Aust.* **1972**, *18*, 419–422. [[CrossRef](#)]
70. Nenna, M.-D. Les artisanats du verre et de la faïence: Tradition et renouvellement dans l'Égypte gréco-romaine. In *L'Apport de l'Égypte à l'Histoire des Techniques: Méthodes, Chronologie et Comparaisons*; Mathieu, B., Meeks, D., Wissa, M., Eds.; Institut Français d'Archéologie Orientale: Cairo, Egypt, 2006.
71. Myśliwiec, K. Tell Atrib field journal. Unpublished work, 1992.
72. Kaczmarczyk, A.; Nenna, M.D. Analyses de faïences égyptiennes d'époque hellénistique et romaine conservées au musée du Louvre. In *Alexandrina 4, En l'Honneur de Mervat Seif el-Din*; Empereur, J.Y., Ed.; Centre d'Études Alexandrines: Alexandria, Egypt, 2014.
73. Thompson, H.A. Two Centuries of Hellenistic Pottery. *Hesperia* **1934**, *3*, 311–476. [[CrossRef](#)]
74. Tite, M.S.; Freestone, I.; Molera, J.; Vendrell-Saz, M.; Wood, N. Lead glazes in antiquity—methods of production and reasons for use. *Archaeometry* **1998**, *40*, 241–260. [[CrossRef](#)]
75. Myśliwiec, K. Tell Atrib field journal. Unpublished work, 1991.

76. Kołodziejczyk, K.; Łajtar, A.; Pawlikowski, M. Fragments d'enduits peints de Tell Atrib. *Etudes Trav.* **1999**, *18*, 99–160.
77. Południkiewicz, A. Arts and crafts workshops in Ptolemaic Athribis (Egypt). In *De la Gaule à l'Orient Méditerranéen. Fonctions et Statuts des Mobiliers Archéologiques dans leur Context*; Ballet, P., Lemaître, S., Bertrand, I., Eds.; Presses Universitaires de Rennes, IFAO: Rennes, France, 2018; pp. 317–324.
78. Bontempi, E.; Benedetti, D.; Massardi, A.; Zacco, A.; Borgese, L.; Depero, L.E. Laboratory two-dimensional X-ray microdiffraction technique: A support for authentication of an unknown Ghirlandaio painting. *Appl. Phys. A* **2008**, *92*, 155–159. [[CrossRef](#)]



© 2020 by the authors. Licensee MDPI, Basel, Switzerland. This article is an open access article distributed under the terms and conditions of the Creative Commons Attribution (CC BY) license (<http://creativecommons.org/licenses/by/4.0/>).